Stony Brook University

Studies of Auxetic Foam and Bridge Deformation Using Digital Speckle Photography

A Thesis Presented

by

Jiandong Yu

to

The Graduate School
in partial fulfillment of the
Requirements
for the degree of

Master of Science
In
Mechanical Engineering

Stony Brook University
December 2010

Stony Brook University

The Graduate School

Jiandong Yu

We, the thesis committee for the above candidate for the Master of Science degree, hereby recommend acceptance of this thesis.

Fu-pen Chiang - Thesis Advisor
Distinguished Professor and Chairperson, Mechanical Engineering Department

Oscar Lopez-Pamies – Chairperson of Defense
Assistant Professor, Mechanical Engineering Department

Chad Korach
Assistant Professor, Mechanical Engineering Department

This thesis is accepted by the Graduate School

Lawrence Martin
Dean of the Graduate School

Abstract of the Thesis

Studies of Auxetic Foam and Bridge Deformation Using Digital Speckle Photography

by

Jiandong Yu

Master of Science

in

Mechanical Engineering

Stony Brook University

2010

The mechanical properties of auxetic (negative Poisson's ratio) foam are studied and reviewed with different experimental methods. Developments in design, manufacture, test and analysis of auxetic foam and related composites are presented. Auxetic foam can be made by open-cell conventional PVC foam, through volumetric compressing and heating process successively. When cooling down to room temperature, the cellular micro structure of PVC foam has been turned out to be re-entranted, which means the ribs of each cell of the foam are protrude inward permanently due to the external mechanical and thermal effects. The new re-entranted structure opens out many interesting and meaningful values. In this thesis, the most updated research in auxetic foam is studied experimentally. Stress-strain relationship and energy dissipation properties are presented through uniaxial loading and cyclic loading tests; force-deflection relationship and shear failure resistance behaviors are carried out through three

points bending test of sandwich beam with auxetic foam core. Meanwhile, compared with conventional foam, advantages of auxetic foam are presented in several aspects as well.

Additionally, a static deflection analysis of a wood bridge is analyzed by DSP and some correlation results are presented in order to do research of aging infrastructures. A truss bridge is structured with commercially available wood planks made of pine. One facet surface of the bridge is painted with a thin coat of retro-reflective paint and illuminated by two 200w flood light. The painted surface of the bridge was photographed before and after the application of static load. Each digital image of the bridge is subdivided into sub-images of 128 ×128 pixel arrays and then "compared" in CASI. The result of a displacement vector map of the entire bridge is verified by Finite Element Method. At last, the strain distribution of main beam is shown and compared with the values of strain gages. The correlation results show that the DSP technique and CASI methods are suitable for the study of these two projects mentioned above. Some future's works also listed.

An optical technique called Digital Speckle Photography (DSP) is used as the analyzing method to measure 2-D or 3-D displacement and strain fields in micro or macro-scale, through which an entire structure deformation pattern and strain distribution from a small foam surface to a big bridge structure facade can be mapped simultaneously in a single step. DSP is an easy setup and the data can be obtained in semi-real time. The displacement of the random features and structures that are often present on many engineering surfaces when viewed in a microscope or CCD camera are measured with the DSP system, followed by an image correlation method - Computer Aided Speckle

Interferometry (CASI). In this thesis, the background and the application of the DSP and the algorithms of CASI are introduced.

Table of Contents

List of Figures

ACKNOWLEDGEMENTS

First and foremost, I offer my sincerest gratitude to my advisor, Dr. Fu-pen Chiang, who has supported me throughout my thesis with his patience and knowledge whilst allowing me the room to work in my own way. Without him, this thesis would not have been completed or written.

I attribute the level of my Master degree to Mr. Ta Yung Hsu's encouragement and instruction. He has prepared me with everything I know about experimental mechanics, which I have used to produce both my results and this thesis.

In my daily work, I have been blessed with a friendly and cheerful group of fellow students. Besides, the Department of Mechanical Engineering has provided the support and equipment I have needed to produce and complete my thesis, and the Navy has funded my studies.

Finally, I thank my lovely wife - Hao, for supporting me throughout all my studies at University, and for providing a warm home in which to complete my writing up.

Chapter 1 Introduction

1.1 Scope of research

In this thesis, two projects are investigated and some new studies are presented. At first, some new properties and performance of auxetic material are shown, and secondly, full mapping deformation of a bridge is demonstrated.

Auxetic material has an unusual and interesting property of having a negative Poisson's ratio. When it is loaded in uniaxial tension, it expands; when loaded in uniaxial compression, it shrinks, laterally. This particular phenomenon gives rise to a variety of unusual mechanical behaviors when auxetic material is subjected to the external force. Auxetic material was found about 100 years ago, but some special attention was given recently only. The earliest man-made auxetic foam was first manufactured in 1987 by Lakes [1]. Subsequently, many researchers have ventured into the field [2-8]. Auxetic foam has several advantages over the conventional ones in many industrial applications, such as aerospace, automotive, ship-building, consumer goods, and so on. For example, an auxetic thin plate deflects much less than a conventional plate for a given load [9]; it can reduce acoustic noise due to its lower cut-off frequency [10]; it resists indentation and has lower velocity impact damage [11]; when bended it deforms synclastically rather than anticlassically thus rendering it ideally suitable for forming into convex-convex surfaces [12]. Furthermore, it has higher shear failure resistance due to the larger shear modulus. In this thesis, several research works have been done for unveiling these special properties. We characterize these mechanical properties of Auxetic PVC foam by an optical measurement method - Digital Speckle Photography (DSP) [12].

DSP method is a very important step in the evolution of speckle techniques. It keeps all the advantages of the speckle photography but requires neither photograph development nor fringe pattern analysis. In digital speckle method, the phase gradients and the position of phase objects can be determined by the speckle displacements obtained defocusedly. The speckle patterns are reconstructed and directly refocused digitizedly into grey levels, through use of the algorithm – Computer Aided Speckle Interferometry (CASI), these patterns can be analyzed and the speckle displacement fields can be calculated. This process can be done either by spatial or spectral analysis. [13]

Digital Speckle Photography can be used to investigate deformation of large structures, such as bridges. Most bridges in this country are aging and require frequent and thorough inspection. However, the current maintaining techniques are too tedious and low efficiency. Moreover, the current technical methods can only capture a small part of the bridge at a time. Now it is necessary to develop a new technique by employing Digital Speckle Photography, whereby the entire bridge deformation pattern can be mapped simultaneously in a single step. And the technique can zoom to a local region and map the local strain distribution in detail. The DSP system does not need expensive equipment and is easy to set up. All of the data can be obtained in semi-real time analysis. In this thesis, a wooden truss bridge was built using standard wood strips and DSP method is applied to investigate the entire bridge deformation.

The aim of this thesis is to use Digital Speckle Photography (DSP) technique to study the mechanical properties of auxetic foam, and the full mapping of deformation of bridge under static loading conditions. The thesis is organized in four chapters, starting

from the conceptions of speckle technique, principles of DSP technique, and algorithms of Computer Aided Pattern Interferometry (CASI), then introduction of auxetic foam, as well as background of inspection of aged bridge, is described and its applications are presented detailedly.

In chapter 2, some prior works, such as uniaxial test, shear test, impact test, which done by the previous students are briefly introduced. Then the manufacturing process of auxetic foam, new tests such as three points bending test, cyclic loading test and fatigue test are presented. Several mechanical properties of auxetic foam are described.

In chapter 3, start from some prior work done by other people, the procedures of building the bridge are demonstrated. Static deflection analysis of the wood truss bridge is also shown. The results are compared with Finite Element Method (FEM). On the other hand, the strain distribution of the local main beam is also presented and analyzed.
In chapter 5, conclusion will be presented and discussion is provided. The results from the DSP technique show that this method is suitable and good for the study of optical-mechanical measurements.

1.2 Speckles and Digital Speckle Photography (DSP)

A speckle is nothing but a random array of dots or spots with a certain size, shape and intensity. It is formed by the interference of two or more rays of coherent light reflecting from diffuse surface of a specimen. Thus each point on the object's diffuse surface acts as a light source with rays propagating radically outward in all directions. The unique properties of a specific speckle are due to local microscopic surface imperfections on the specimen. If the surface of the specimen undergoes a deformation

speckles move. Fig 1.1 shows a typical laser speckle pattern. Since the speckle pattern is caused by random interference of light, it acts as a grid in all directions printed on the object's surface. By comparing the speckle patterns before and after the deformation, displacements and strain on the surface can be determined.

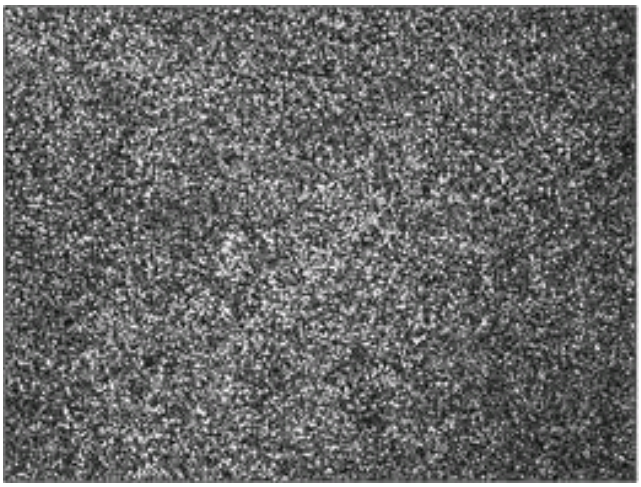

Fig 1.1 A typical laser speckle pattern

The use of a random speckle pattern for quantitative displacement and strain measurement represents a major milestone in the art of experimental mechanics. And its origin can be traced back to the paper by Burch in 1968 [17]. However, its development owes a large part to the advent of laser and laser related techniques such as holographic interferometry and speckle interferometry [18]. In the earlier stage of the development laser speckle, which is the natural consequence of coherent illumination, was almost exclusively employed [19]. Later white light speckle [15, 20] or other non-coherent speckle patterns [21] are used. With the advent of high resolution digital camera and high computational power personal computer the old fashioned photographic recording and optical processing are replaced by digital recording and numerical processing, thus the birth of digital speckle photography (DSP) [14, 22].

Digital Speckle Photography (DSP), (sometimes referred to as Electronic Speckle Photography, (ESP)) is the digital version speckle photography. The relatively low complexity in the hardware for a basic DSP system is shown in Fig 1.2. The object is illuminated by an expanded laser beam or simply by white light. The registration of the speckle pattern is made by digital recordings of the object and the evaluation process is performed on a computer.

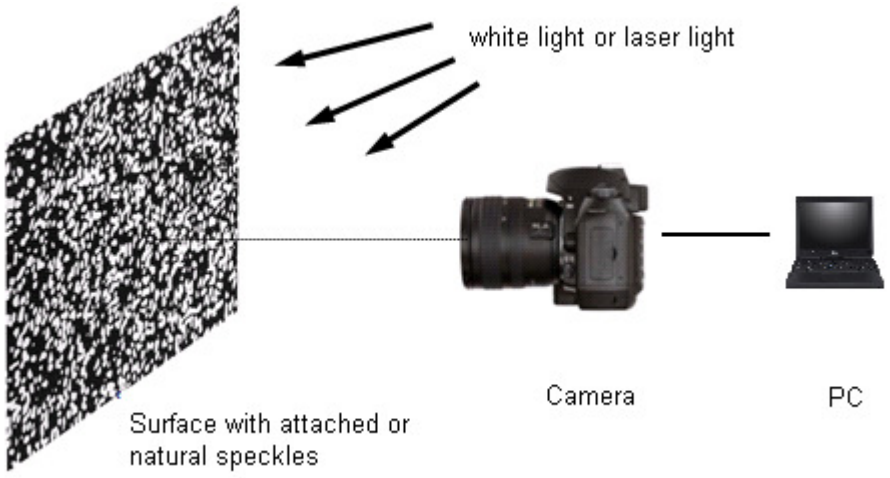

Fig 1.2 Schematic of a simple DSP system

Since DSP follows the motion of the speckle pattern at all parts of the object, the absolute motion of the speckle pattern in the plane of the detector is obtained. The experimental results of the in-plane motion of a copy paper exposed to an increased humidity are shown in Fig 1.3. This figure highlights in DSP, the absolute values of both the in-plane deformation components can be obtained directly. On the other hand, in general, DSP method presents higher spatial resolution and accuracy when compared to other technique such as Digital Speckle Interferometry. In the literature, a number of DSP systems have been presented by many researchers, including Chen and Chiang [16, 25], Sjodahl [26].

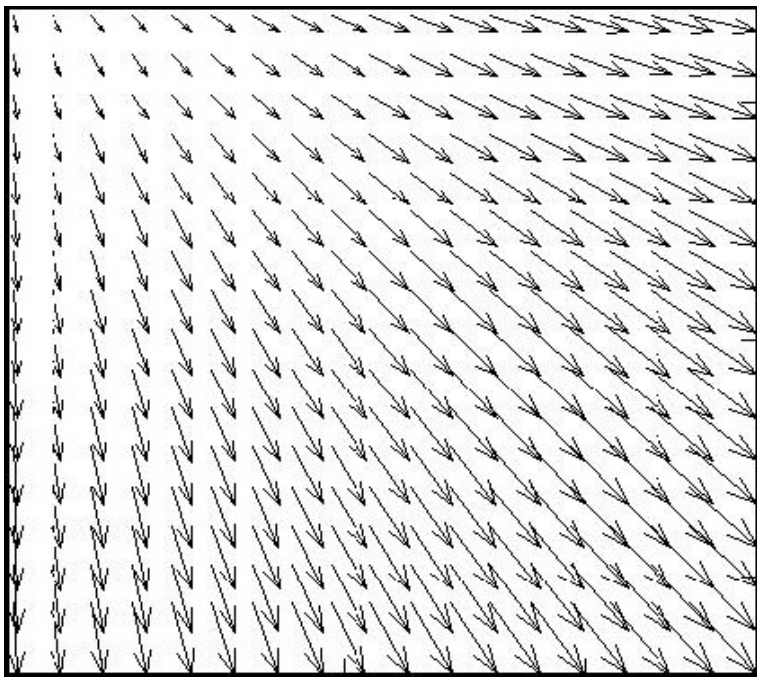

Fig 1.3 Speckle displacement field

The advantages of DSP over classical Speckle Photography are not only the easiness and fastness of using the system. With electronic detection, individual frames are stored in the computer and a whole sequence of images, registered with the same or varying illumination directions, may be captured without altering the experimental set-up. The images being stored on different frames, first of all, allows the use of a digital cross-correlation algorithm rather than the auto-correlation approach used in traditional Speckle Photography (Young's fringe method) [26]. This eliminates the directional ambiguity. Secondly, each image may be manipulated prior to the analysis, which opens up further possibilities, such as subtracting the mean intensity value.

In Digital Speckle Photography, at least two images are recorded and analyzed. One image is taken before and another image is recorded after a change in the specimen. A computer program is used to analyze these images. Each image will be processed digitally and divided into many small sub-images. And then a numerical cross-correlation

step is performed and characterized for each sub-image pair. Finally the average displacement and deformation are obtained for each pair. On the spectral domain, the correlation technique will be using Computer Aided Speckle Interferometry (CASI) [27]. While it provides comparable range and sensitivity with the digital speckle correlation, this technique had a much higher computing efficiency and will be discussed more detailed in the next section.

1.3 Computer Aided Speckle Interferometry (CASI)

Using a random pattern for quantitative displacement or deformation measurement is a major milestone in the history of experimental stress and strain analysis. Heretofore, measurement of deformation is done by using a regular geometric pattern (grating, grid, optical markers, fringes, etc.) whose deviation from the norm is used as a gauge of deformation. The speckle methods, on the other hand, employ a random dot pattern, such as speckles, as a measuring gauge. Quantitative measurement is not done by direct comparison, rather it is obtained by maximizing the cross correlation between the random pattern before and after displacement or deformation. In the following, a Digital Speckle Photography technique will be described, whereby the displacement sensitivity and spatial resolution can be varied by judiciously selecting the proper speckle size and recording magnification.

A random light intensity distribution of any sort can be considered as a speckle pattern, which may be naturally present or artificially created on the surface (or interior) of a specimen. The speckle pattern is digitally recorded sequentially before and after deformation and processed using a specially designed algorithm called Computer Aided

Speckle Interferometry (CASI). The essence of CASI is described in the following. Two speckle patterns, one before and one after deformation, are first segmented into subimages of 32x32 pixels, for example, and the displacement of all points within a subimage is assumed to be constant.

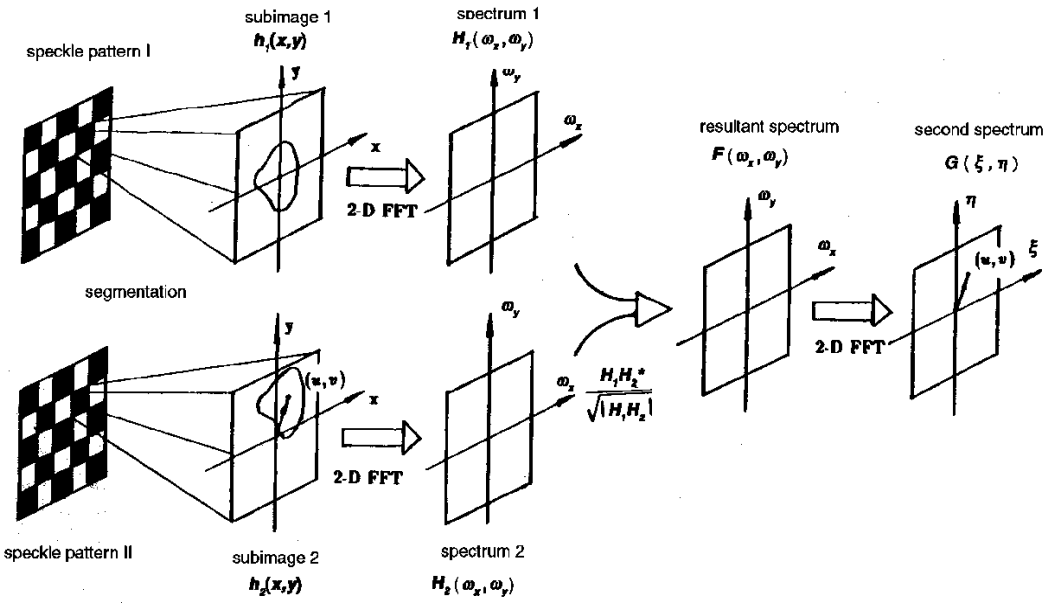

Fig 1.4 Schematic of CASI for calculating displacement vectors

The corresponding subimages of the two recordings are "compared" via a two-step FFT (Fast Fourier Transform) process to find the displacement vector. Fig 1.4 is the schematic of the CASI process. In Fig 1.4, $h_1(x, y)$ is the complex amplitudes of the light disturbance of a generic speckle subimages before deformation and $h_2(x, y)$ is nothing but the original speckle pattern with displacement components added, i.e.:

$$h_2(x, y) = h_1 [x - u(x, y), y - v(x, y)] \quad (1)$$

where u and v are the displacement components along the x and y directions, respectively, of the subimage "point". The procedure now is applied a FFT to both h_1 and h_2.

$$H_1(\omega_x,\omega_y) = \Im\{h_1(x,y)\} \quad (2)$$

$$H_2(\omega_x,\omega_y) = \Im\{h_2(x,y)\} \quad (3)$$

Then, a numerical "interference" between the two speckle patterns is performed on the spectral domain as follows,

$$F(\omega_x, \omega_y) = \frac{H_1(\omega_x, \omega_y) H_2^*(\omega_x, \omega_y)}{\sqrt{|H_1(\omega_x, \omega_y) H_2(\omega_x, \omega_y)|}} =$$

$$\sqrt{|H_1(\omega_x, \omega_y) H_1(\omega_x, \omega_y)|} \exp\{j[\phi_1(\omega_x, \omega_y) - \phi_2(\omega_x, \omega_y)]\} \quad (4)$$

where $\varphi_1(\omega_x, \omega_y)$ and $\varphi_2(\omega_x, \omega_y)$ are the phases of $H_1(\omega_x, \omega_y)$ and $H_2(\omega_x, \omega_y)$, respectively, and * denotes complex conjugate.

$$\phi_1(\omega_x, \omega_y) - \phi_2(\omega_x, \omega_y) = 2\pi(u\omega_x + v\omega_y) \quad (5)$$

Finally, a halo function is obtained by a second FFT,

$$G(\xi, \eta) = \Im\{F(\omega_x, \omega_y)\} = \bar{G}(\xi - u, \eta - v) \quad (6)$$

which is an expanded impulse function located at (u, v) of the ξ and η plane. Thus, by detecting the crest of this impulse function, the displacement vector represented by the cluster of speckles within the subimage is uniquely determined. Strains are then calculated using an appropriate strain-displacement relation. By recording the speckle image at incremental loads, strain of almost any finite magnitude can be obtained. And this is the technique used in all the subsequent discussions on displacement and strain measurement. At macroscales the texture of the foam cells themselves services as the speckle pattern. At microscales, the glass beads spread on the surface of bridge with micron size are to serve as speckle patterns. The speckle patterns at different stages of specimen deformation are recorded digitally via a CCD camera, an optical microscope. Processing is performed using the CASI algorithm. The interface of CASI is shown in the next figure.

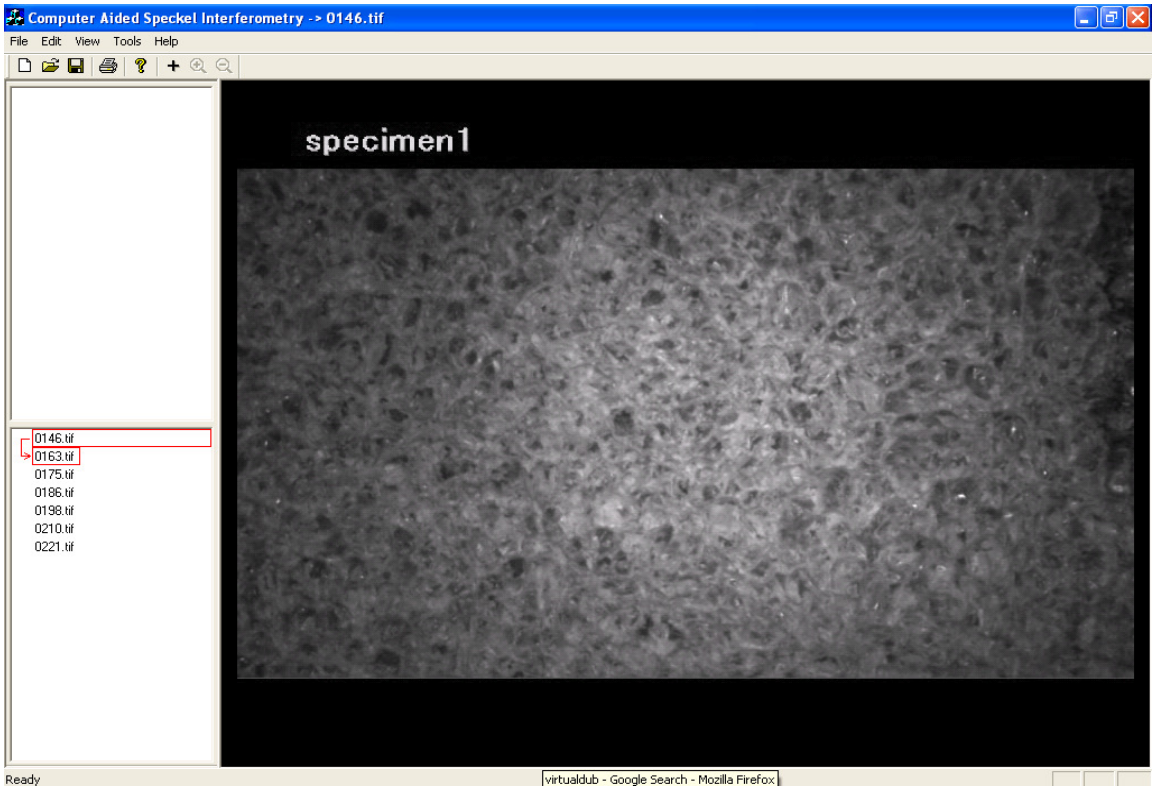

Fig 1.5 User graphic interface of CASI

1.4 Introduction of Auxetic Foam

Poisson's ratio and Auxetic foam

Poisson's ratio is defined as the negative of the ratio of the transverse normal strain divided by the longitudinal strain for uniaxially loaded specimen. Most common materials shrink transversely when stretched longitudinally, which makes Poisson's ratio of these materials positive. However, a novel material named negative Poisson's ratio foam (also called, Auxetic foam, anti-rubber, dilatational, etc.) was manufactured by Lakes in 1987 [1]. The term *auxetic* derives from the Greek word αὐξητικός (auxetikos) which means "that which tends to increase". This terminology was coined by Professor

Ken Evans of the University of Exeter [2]. The auxeticity of the material is defined by the foam structure with re-entrant cell shapes Fig 1.6.

Fig 1.6 Idealized re-entrant unit cell produced by symmetrical collapse of a 24-sided polyhedron with cubic symmetry [1]

Till now, amounts of auxetic materials have been discovered, manufactured, tested and theoretically predicted, such as polyurethane and polyethylene foams prepared by Lakes [9-11], Evans [27].

When the vertical links are applied with tension, the cell of Fig 1.5 will be unfolded and expanded laterally. The actual cell structure also contains ribs, which are bent and protruded into the cells. The three-dimensional unit cell was modeled as an idealized polyhedron unit cell of isotropic foam structures [7].

Foams with negative Poisson's ratios were produced from conventional low density open-cell polymer foams (Fig 1.7) by causing the ribs of each cell to be buckled and permanently protrude inward, resulting in a re-entrant structure such as shown in Fig 1.8 [1].

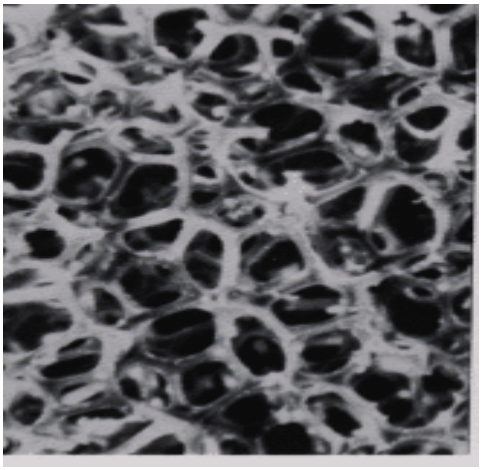

Fig 1.7 Conventional open cell polymer foam. Scale mark: 2 mm. The original shows a stereo pair.

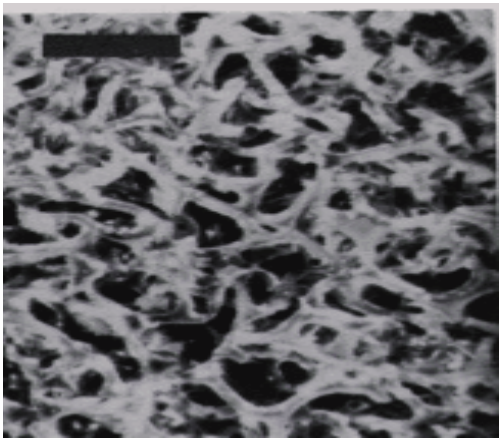

Fig 1.8 Auxetic foam with re-entrant structure. Permanent volumetric compression is a factor of 2.7. Poisson's ratio is -0.6. Scale mark: 2 mm. The original shows a stereo pair.

Umbrella effect

Auxetic foam can be manufactured by conventional foam with triaxial compression and heated to about 135^{o}C and then cool down to room temperature. From Fig 1.6 and Fig 1.7, one typical characteristic is that the micro-structural has been changed from open cell to re-entrant. The new properties of Auxetic foam can be seen as an “Umbrella effect”. Fig 1.9 is a simple sketch of an umbrella.

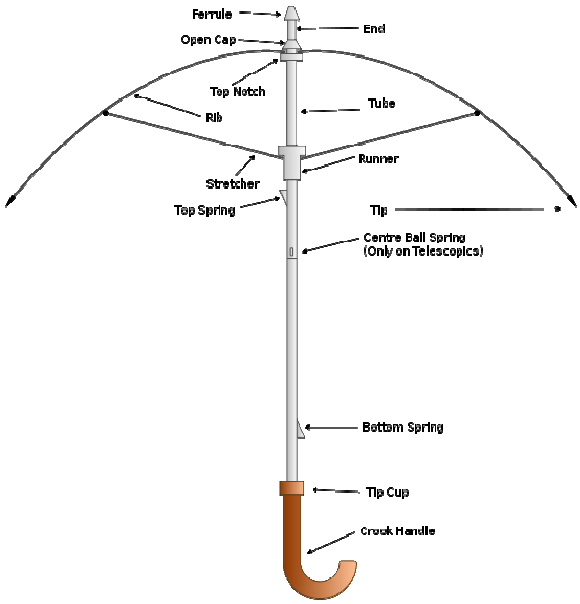

Fig 1.9 Sketch of an umbrella effect [29]

From Fig 1.9, if the ribs are exerted from external force, the runner will be pulled down along the tube, and the umbrella is folded. However, when the runner is pulled up along the tube, the ribs will expand to all ways by the support of each stretcher, and the umbrella opens. The process of opening and folding of umbrella is quite similar to the process of making auxetic foam and the re-entrant effect.

General properties of Auxetic foam

When compared with the conventional foam, the Auxetic foam has more desirable and advantage properties in some applications. It is more impact resistant [1, 31]; it bends into synclastical rather than anticlastical curvature [32]; it has better resistance to shear failure [2] and it is efficient in noise absorption [5]. Sandwich panels made of fiberglass face sheet and Auxetic foam core are increasingly being used as important structural material for ship construction due to its lightweight, and very strong. Moreover, auxetic foam has higher fatigue resistance. All the properties will be investigated in this thesis through experimental studies. The mechanical performance of the auxetic foam has been

buttressed shear test, indentation and impact test, three-point bending test and cyclic loading test.

Applications and significance

Sandwich panels with foam cores have gained substantial importance in marine application for over 60 years to lighten, stiffen, and strengthen the boat structures [33]. The decreased weight helps to increase top speed and acceleration, increase cargo capacity, and reduce operation and maintenance cost. The increased stiffness and strength allow builders to use less skin material resulting in even lower weight structure. The sandwich structure consisting of a foam core and two skins has many advantages including better thermal insulation, improved impact/damage resistance, longer fatigue life, and sound attenuation [34].

The development of new auxetic materials and processing routes in recent years has been accompanied by a number of patent applications and publications from organizations including Toyota, Yamaha, Mitsubishi, AlliedSignal Inc, BNFL and the US Office of Naval Research, all relating to the emerging potential of these materials. It is important to understand interactions within the material structure that give rise to auxeticity, and it is also necessary to keep studying the overall behaviors of these novel materials as pointed out by Lakes.

Auxetic foam has been applied in many other industrial fields. In biomedical industry, it can be made to prosthetic materials, surgical implants, ligament or muscle anchors, and piezoelectric and actuators. In automotive field, Auxetic fiber reinforcements should also enhance the failure properties of composites. It allows the

possibility of maintaining the interface by carefully matching of the Poisson's ratios of the matrix and fiber.

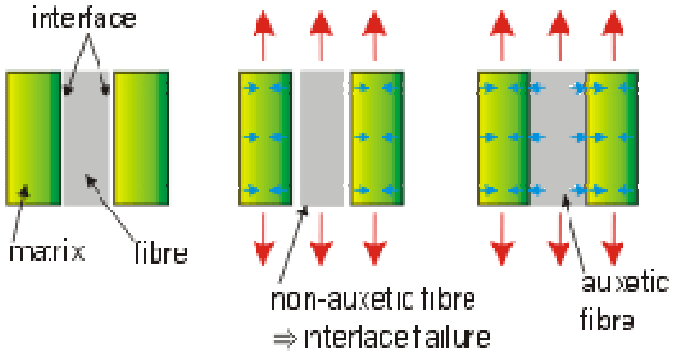

Fig 1.10 Fiber pull-out in composites

1.5 Inspection of Aged bridges

According to the United States Department of Transportation (USDOTs), methods of monitoring the aged bridges are identified to three prevailing types: visual monitoring, measurement, and instrumentation [35]. Visual inspection by human depends on the different training and experience background of the inspectors and crews, which tends to be leading to uneven inspecting conclusions. Measurement is the collection, usually by hand methods or quantitative values during routine inspections, which is tedious and time consuming. Although some instrumental inspection methods, such as acoustic detectors, strain gages or thermal imaging techniques are provided for precise data collection. However these techniques can only be applied to a small portion of the bridge at a time. Mapping the entire bridge using a regional technique is also time consuming and expensive. Typically the failure mode of a bridge tends to start in local (such as the failure of the I35 Minneapolis Bridge in 2007) and then propagates to other regions, finally leading to catastrophe. Thus, it is paramount that a nondestructive evaluation technique should be developed so that the entire bridge can be inspected by a

single glance or observation. And this full field inspection should be maintained as a function of time.

Chapter 2 Studies of Auxetic Foam

2.1 Prior works

Auxetic foam has shown some unique properties: it has less deflection for flat panel. The deflection of a circular plate can be expressed by:

$$d = \frac{3FR^2\left(1-\nu^2\right)}{16Et^3} \tag{7}$$

Here, R is the radius; t is the thickness; E is Young's Modulus, and ν is Poisson's ratio; F is the external force. When the Poisson's ratio approaches -1, the deflection approaches zero [2].

The auxetic foam has less shape distortion, which owns to the higher shear modulus. If G equals to the Measure of resistance to applied shear load:

$$G = \frac{E}{2(1+\nu)} \tag{8}$$

E is Young's Modulus, ν is Poisson's ratio. When ν approaches -1, G approaches infinity.

Prior works are cited in this section which done by other graduate student (G. Uzer, et el.,) [12, 37] is to present some experimental results and basic mechanical properties of Auxetic foam mentioned above. These experiments have been carried out by the author as well.

Displacement vectors distribution

Fig 2.1 shows a typical specimen under uniaxial tension and resulting displacement fields.

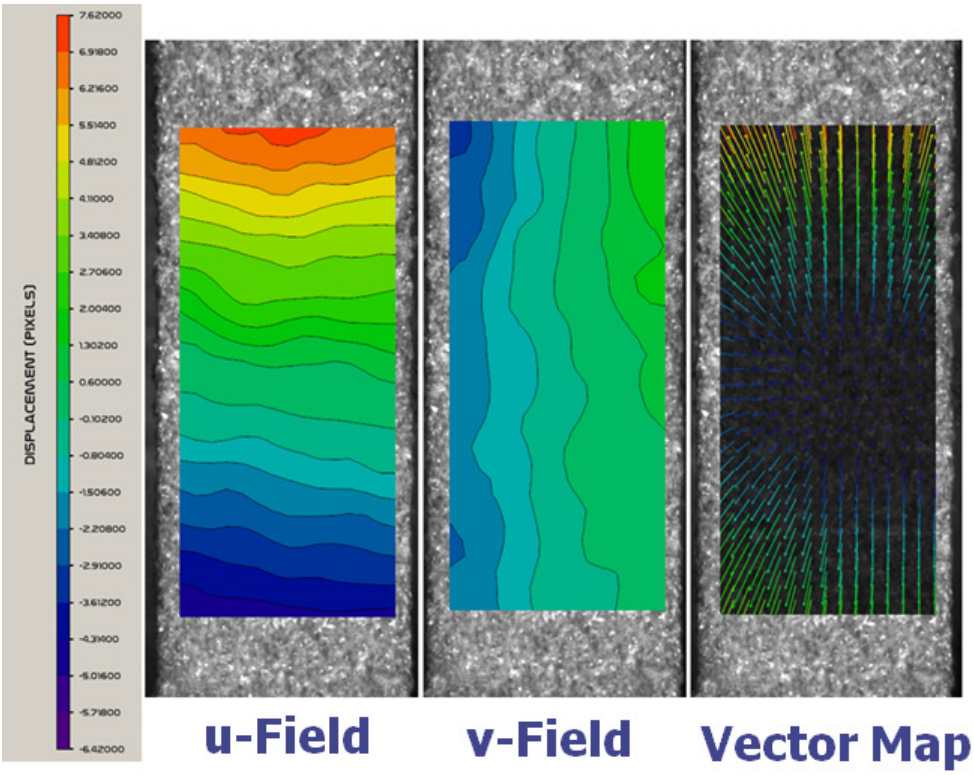

Fig 2.1 Example of displacement fields obtained by CASI. u field, v field and total displacement vector. (Contour Constant is 31μm)

It can be seen clearly of the auxetic behavior from the vector fields that with increasing load, the specimen expands in both directions without much rotation. The contour lines are not ideally straight as would have been. This type of non-uniformity is relatively minor, which is unavoidable due to local variation of the foam's properties resulting from the manufacturing process.

Stress and strain curve

The true stress can be calculated through:

$$\sigma_{true}=F/A_0 \qquad (7)$$

where F is load, recorded by the microtester, A_0 is real time cross section area of the auxetic foam in the viewing area. The results of strain can be computed through CASI as the following method: each image was imported to the CASI and subtracted

consecutively to get the displacement distribution. Then by taking the derivative of the displacement, the strain distribution can be obtained.

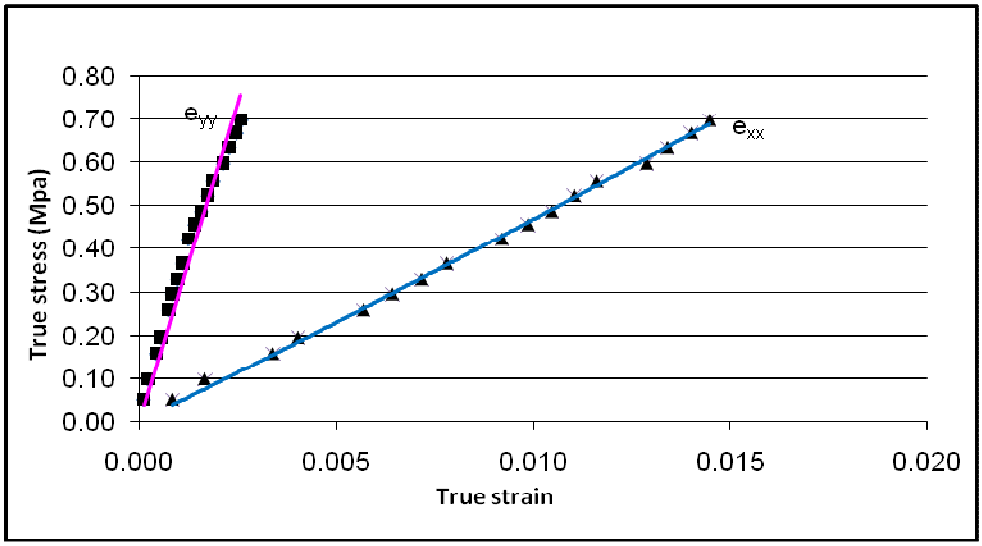

Fig 2.2 Typical stress-strain curves of Auxetic foam

Fig 2.2 is the stress-strain relationship of single piece specimen of auxetic foam under uniaxial tensional loading test. e_{xx} is the true strain aligns with the direction of load, while e_{yy} is the true strain across the direction of the load.

Poisson's ratio effect

Poisson's ratio (ν) is the ratio, when a sample object is stretched, of the contraction or transverse strain (perpendicular to the applied load), to the extension or axial strain (in the direction of the applied load). Poisson's ratio ν is a measure of the Poisson effect.

$$\nu = -\frac{\varepsilon_{trans}}{\varepsilon_{axial}} = \frac{\varepsilon_x}{\varepsilon_y} \tag{8}$$

ε_{trans} is transverse strain (negative for axial tension, positive for axial compression, and ε_{axial} is axial strain (positive for axial tension, negative for axial compression).

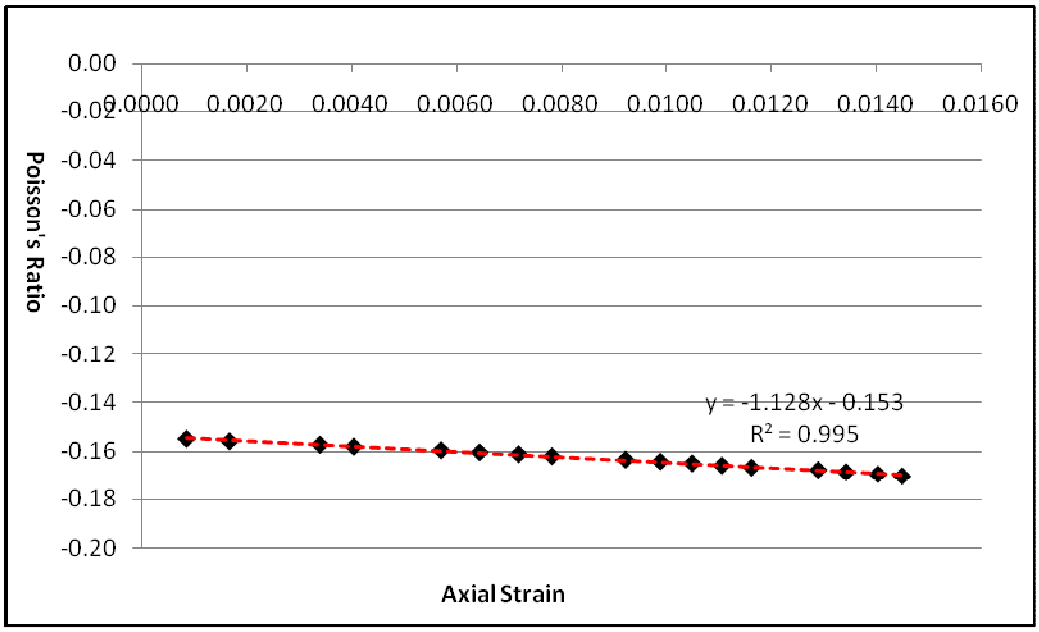

Fig 2.3 resulting of Poisson's effect

In Fig 2.3, the Poisson's ratio here is defined simply as the ratio of transverse strain over the longitudinal strain when loaded in uniaxial tension. This conclusion can be drawn from Fig 2.2 as well. The value of negative Poisson's ratio is about -0.16. Noticed in Fig 2.3, the line stands for the value of Poisson's ratio is not perfect horizontal. This non-uniformity is also unavoidable due to local variation of the foam's properties resulting from the manufacturing process which leads to the non-uniform distribution of Auxeticity of the cubic specimen.

Auxeticity and Volumetric change

Triaxial compression by hydraulic machine is consisted of the manufacturing process from conventional foam to auxetic foam. Typically the global volume will be decreased to about 50% and some local area volume will be changed up to 60%~75%. The Poisson's ratio changes essentially linearly with the volumetric change. The larger the amount of the volumetric change, the larger the negative Poisson's ratio is. This relationship is shown in Fig 2.4.

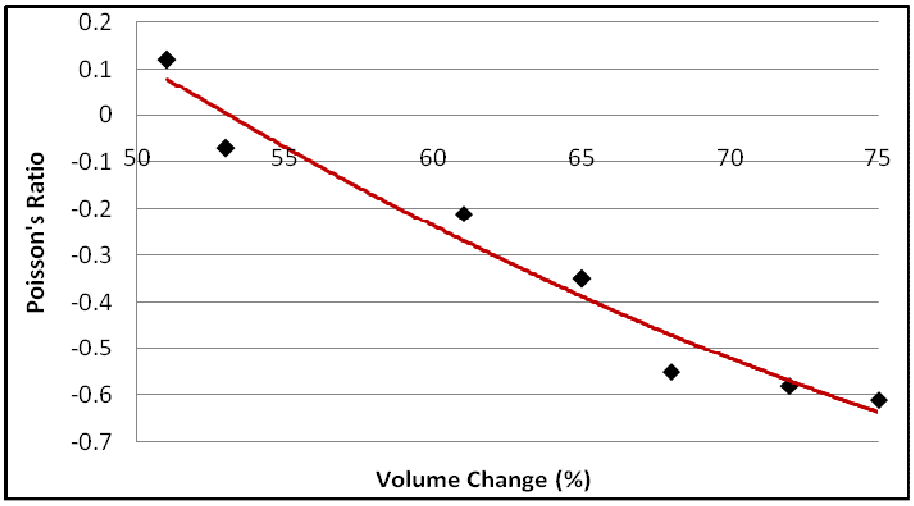

Fig 2.4 Poisson's ratio as a function of volumetric change

Shear Test

Due to the negative Poisson's ratio, auxetic foams will have better shear resistance. An experimental setup was prepared as shown in Fig 2.5.

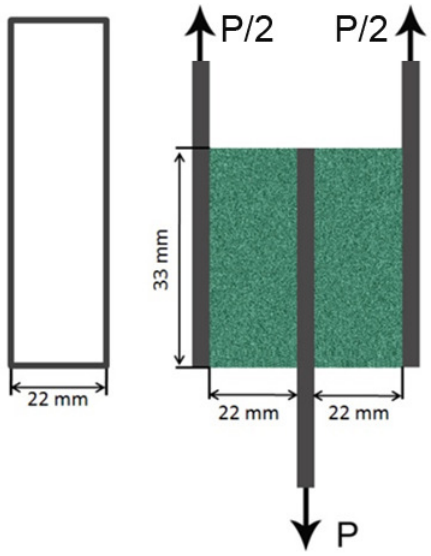

Fig 2.5 Schematic of shear test setup

When the specimen is loaded in tension, foam blocks in both sides will undergo simple shear deformation. The original PVC foam has the following mechanical

properties: Young's Modulus is 90Mpa, Poisson's Ratio is 0.3. Based on the elastic shear modulus equation (8):

The shear modulus equals to 28Mpa. Fig 2.6 shows the deformation field of the test specimen under a load of 300N. Using the displacement fields from the experiment, the shear modulus was 38Mpa on average, which is much greater than the value from conventional foam.

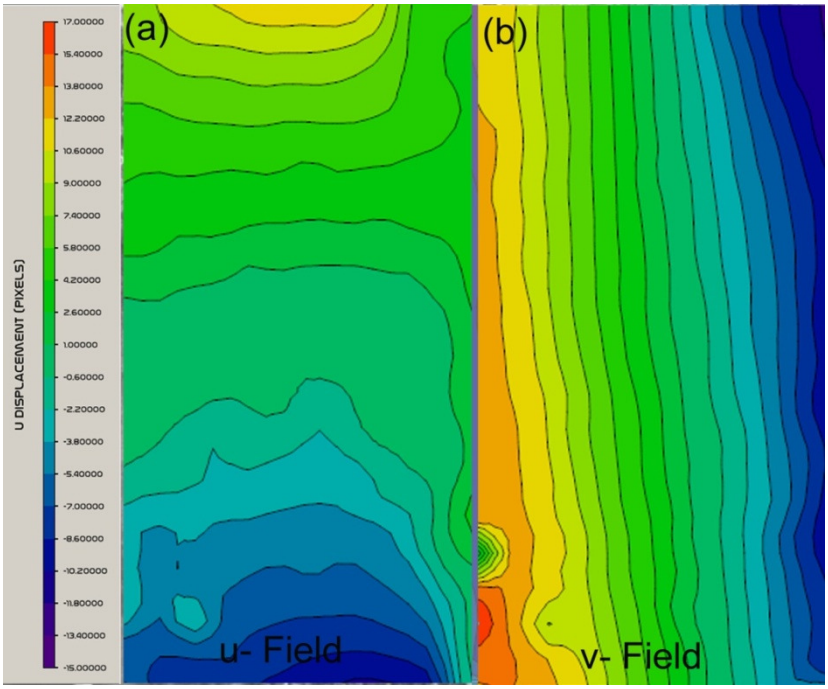

Fig 2.6 Deformation contours of the shear test specimen

Impact test

A low speed impact test was conducted by using a Daisy 105B air gun, with 4.5mm steel bullets in order to investigate the relative impact resistance of auxetic foams as compared to the unprocessed conventional foam, shoot the foam targets. Grids were marked on the surface of the cubic specimen to show the volume change and set the impact sites at different positions with different volume change, which means different Poisson's ratios. Fig 2.7 shows the results of an example specimen. Fig 2.8 (a) shows the

shot spots together with the deformed grids after processing of the foam cube. In Fig 2.8 (b) the triangle marks are the penetrations depth from the impact locations. For this test, the smaller the Poisson's ratio is, the shallower the penetration depths are. Auxetic foam tends to be having higher resistance over the normal conventional foam.

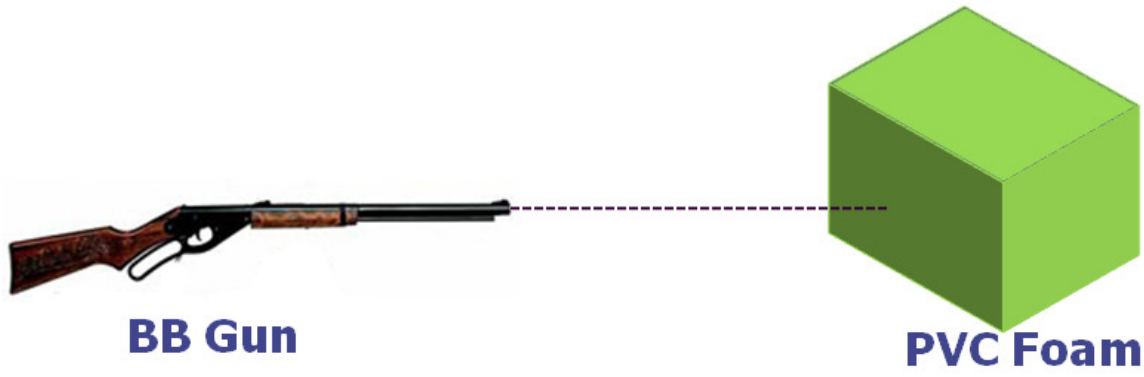

Fig 2.7 Experimental setup of impact test

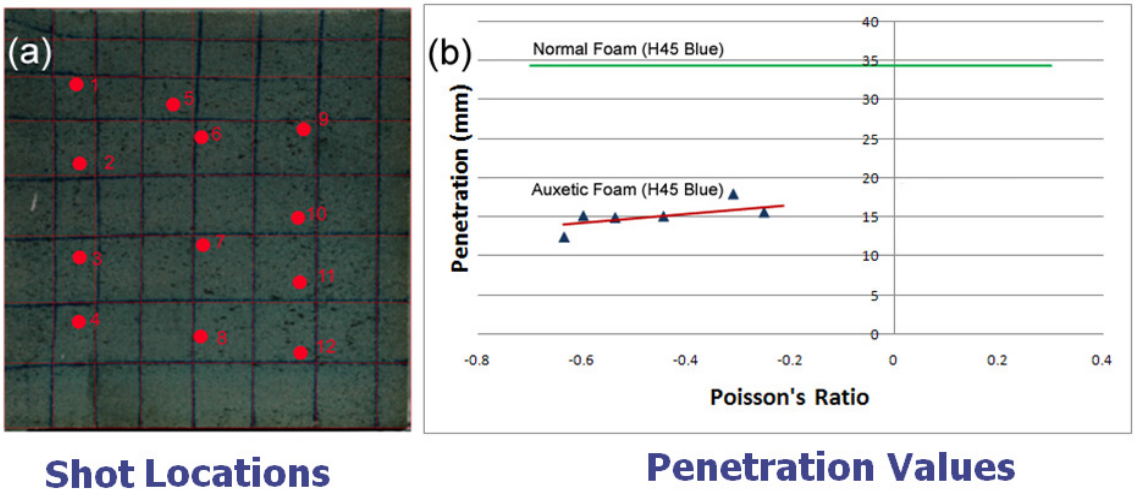

Fig 2.8 Penetration values of the metal bullets into the foam block as a function of Poisson's ratio

Indentation test

An indentation test was carried out with the Auxetic foam to exhibit that Auxetic material tends to have better indentation resistance due to its negative Poisson's ratio, to conventional foam. Indentation experiment was done by a loading frame. The result of

load displacement curves were plotted in Fig 2.9. In this figure the red line represents the result of auxetic foam and the green line represents the result of conventional foam. The comparison clearly shows that the auxetic foam becomes stiffer when the load is increasing, which indicating that area under the indenter tip contracts and shrinks under the load. However, conventional foam starts to be failure after about 30N and the load starts to drop after about 34N. Conclusion can be drawn that the auxetic foam does demonstrate better indentation resistance.

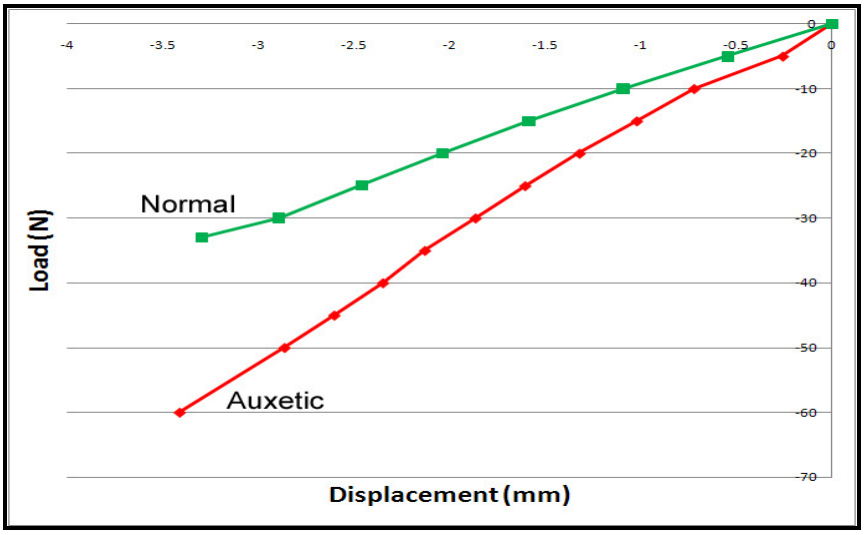

Fig 2.9 Load displacement curves of auxetic and conventional foam

Example of Indentation Area (IA) was created by the indenter shown in Fig 2.10. The Indentation Area (IA) was review under microscope. On the left is the conventional foam, the diameter of its IA is about 12mm when the external load is 35N. Right is the auxetic foam, whose diameter of IA is about 7.5mm when the external load is 60N. The reason is that because the micro structural of auxetic foam has been re-entranted, which induces more resilient than conventional foam when it is compressed.

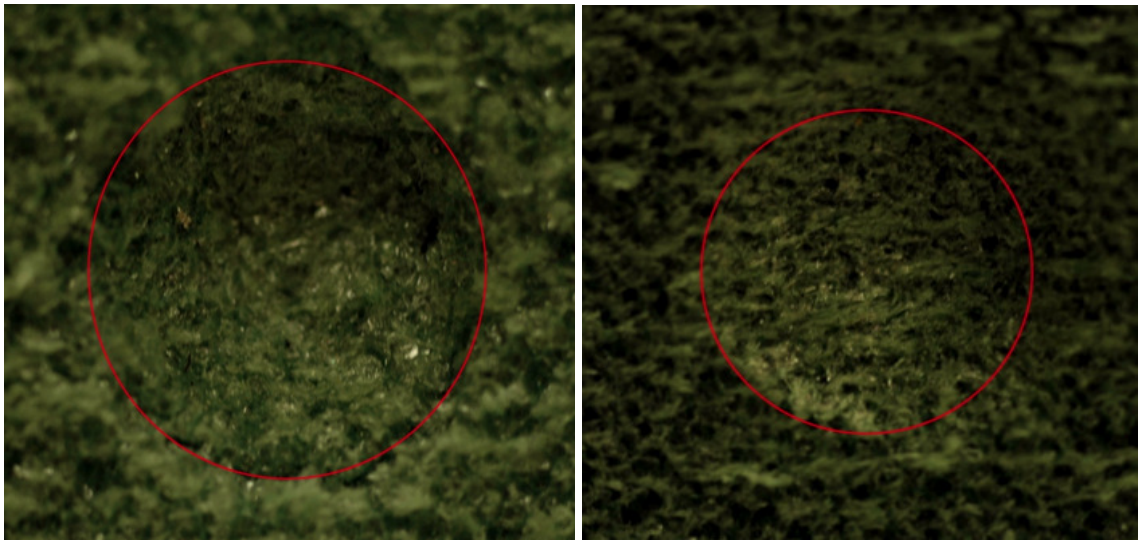

Fig 2.10 Indentation area under the view of microscope
Left: Conventional Foam, IA: d=12mm at 35N; Right: Auxetic foam, IA: d=7.5mm at 60N

Cyclic loading test

Cyclic loading test was performed and the results were compared between using CASI and LVDT. The results obtained by LVDT show a large amount of plastic deformation, while the results by CASI remain elastic with little permanent plastic deformation.

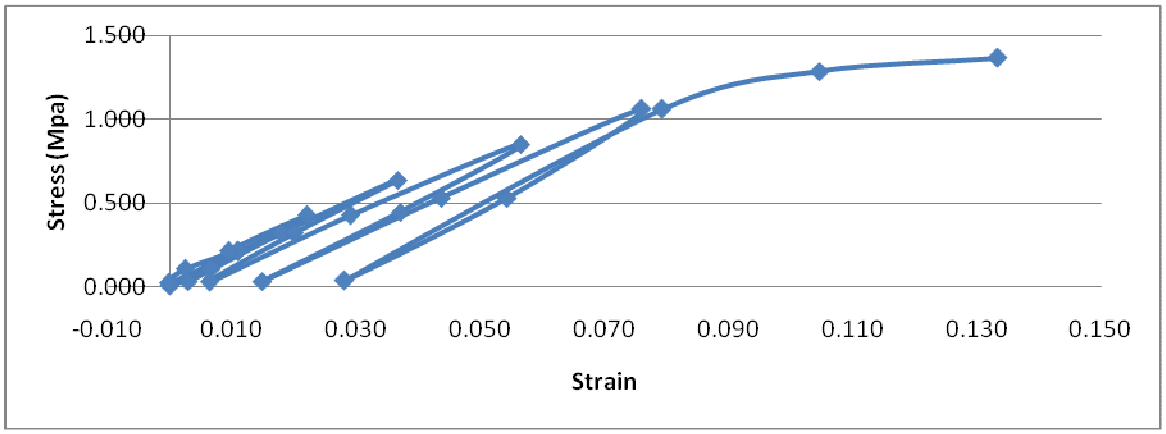

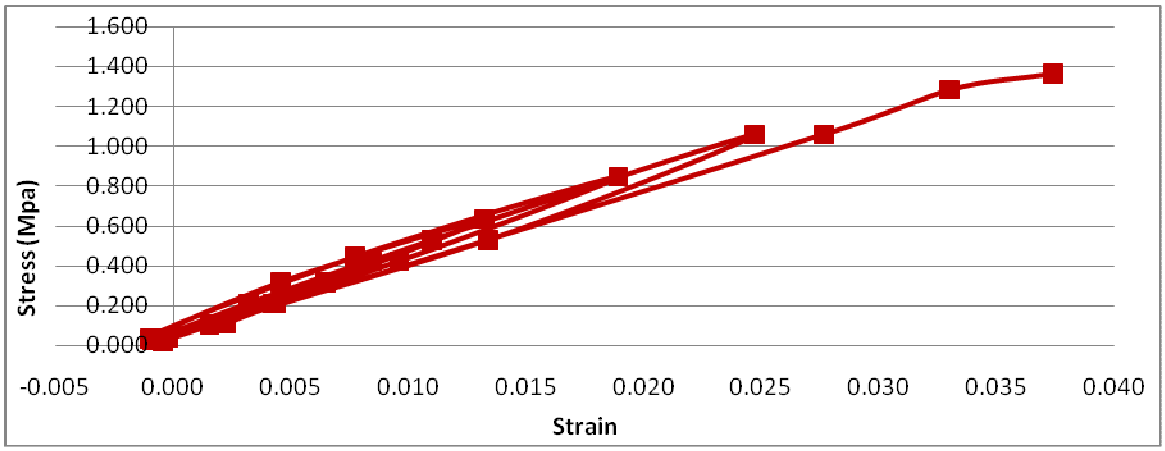

Fig 2.11 Deformation of the conventional foam (upper) and auxetic foam (lower)

2.2 Manufacturing Process of Auxetic Foam

A conventional PVC foam cubic sample with its size 75mm×75mm×75mm was first cut. The mechanical properties of PVC foam are: size of the foam cell is about 50 μm, the tensile strength is about 0.6 MPa, Young's modulus is 90MPa, and the density is 44.3kg /m^3. Auxetic foam can be manufactured by the following steps:

(1) Compressing conventional PVC foam in three dimensions sequentially by clamped it in an aluminum mold (Fig 2.12) and then compressed by a hydraulic press triaxially. The manufacturing scheme is presented in Fig 2.13.

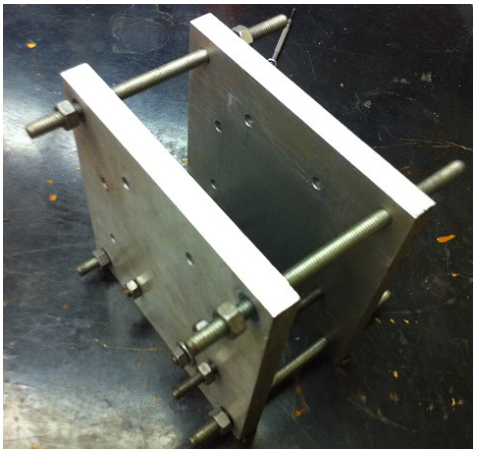

Fig 2.12 An aluminum mold for compressing the conventional foam triaxially

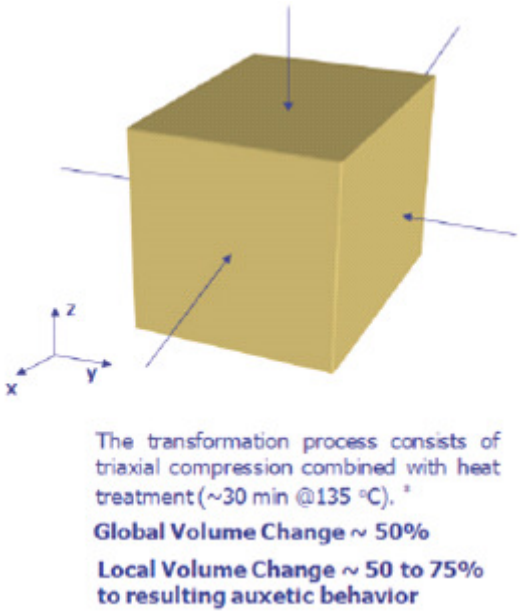

Fig 2.13 Manufacturing scheme of converting conventional foam to Auxetic foam

(2) The aluminum mold with the sample foam inside was heated to about 135^{o}C in a furnace and kept at that temperature for about 15~30 minutes.

(3) The aluminum mold was allowed to cool down to room temperature (23 ^{o}C) and the resulting foam became auxetic.

Some physical phenomenon should be noted here: the global volume reduction of the produced foam was about 50% from the original sample, but the local volume change varies up to 75%. After compression and heat treatment, open cells become smaller and buckled and crushed inward. Indeed it is this inward deformation, called re-entrant structure here, which gives rise to the auxetic behavior. It should be noted that this type of manufacturing process can also be applied to many different foams such as copper. The schematic of the micrographs of the conventional and auxetic foams and the manufacturing process are shown in Fig 2.14.

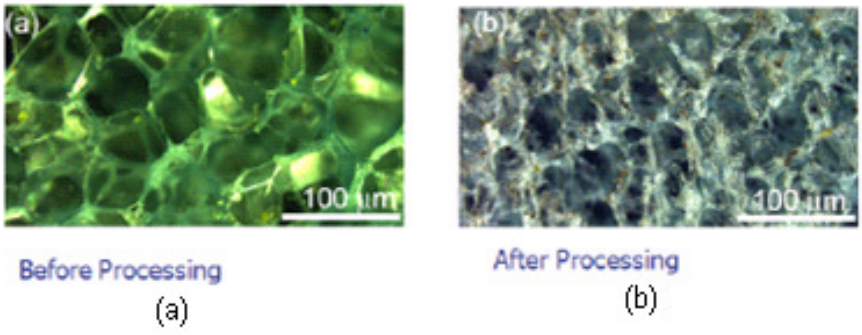

Fig 2.14 Cell image of foam material (a) before processing, (b) after processing

In order to measure the change of volume and deformation that the specimen experienced during the manufacturing process, each surface of the specimen block was marked onto a 10mm×10mm grid (Fig 2.15). The purpose of which is to track the global deformation of the specimen and selected local regions that have uniform deformation. During the manufacturing process, the surface layer of the foam became stiffer than the interior of the foam because the surface layer was exposing to the heat source directly. To eliminate this heterogeneity, the top surface layers were cut off from the foam block. Then, a layer about 10mm in thickness was cut off from one of the surfaces of the fabricated foam to produce coupon specimens.

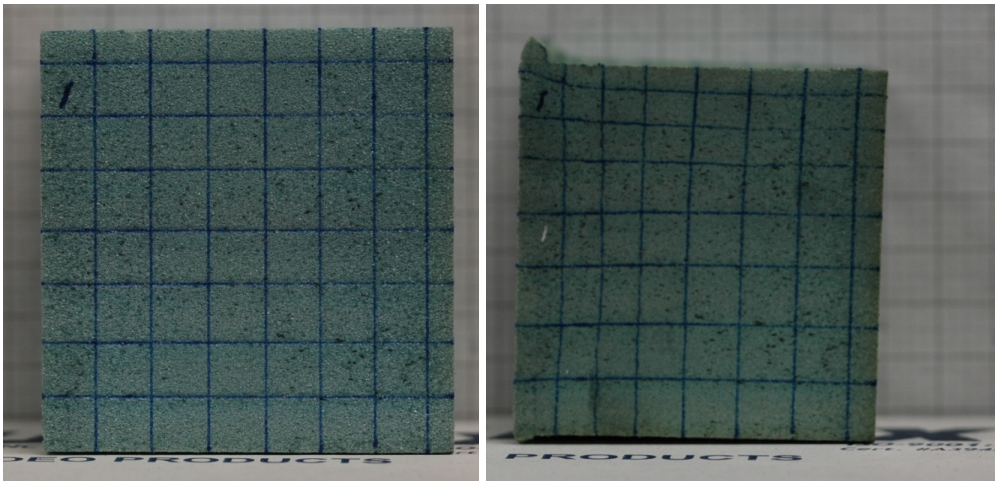

Fig 2.15 Grided surface of conventional foam (left) and auxetic foam (right)

2.3 Experimental Setup

Uniaxial tensile and cyclic test

Coupon specimens were cut from processed foam about 7mm×10mm×65mm in size and tested under uniaxial tensile loads. A typical example of the specimen dimensions and its corresponding optical micrograph of viewing area are shown in Fig 2.16.

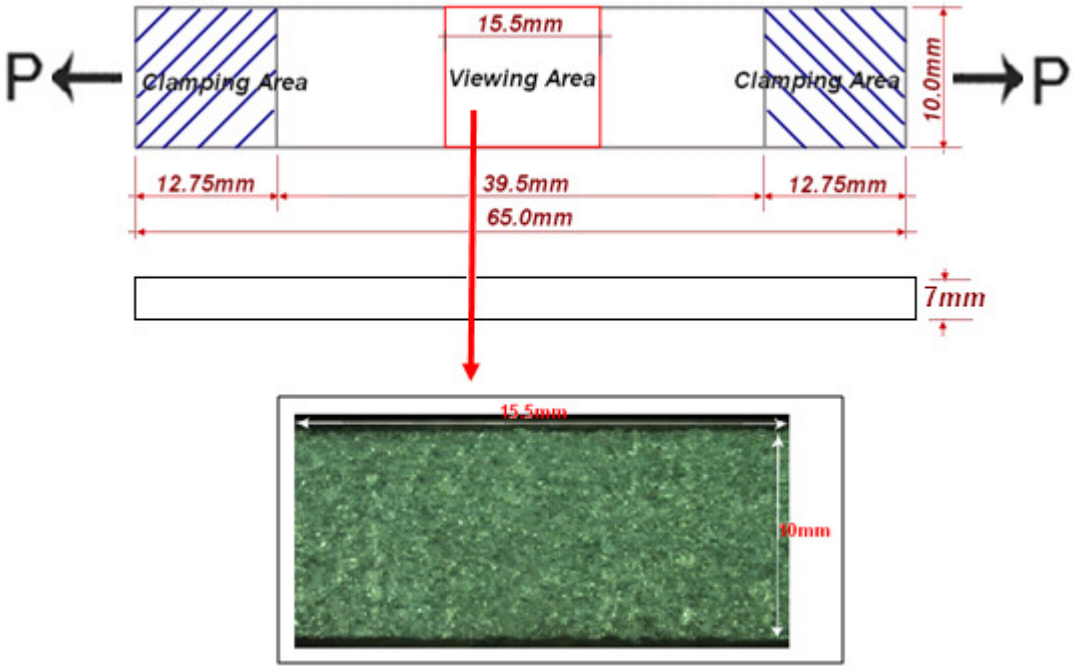

Fig 2.16 Coupon specimen of uniaxial test and its viewing area under microscopy

Bending test specimen

Coupon specimens cut from auxetic foam about 63.25mm ×21.02mm×12.55mm in size were prepared for bending test. The distance between two supports is about 50.1mm. The core material was bonded by glass fiber layers with Epoxy. The geometry of specimen and the schematic of bending test are shown Fig 2.17.

Optical system

The Specimens will be tested first and then analyzed by DSP. A VHX-100 digital optical microscope (Fig 2.18) was used to record the speckle pattern as the load was being applied quasi-statically by a servo controlled microtester (Fig 2.19) at a constant rate 2mm/min.

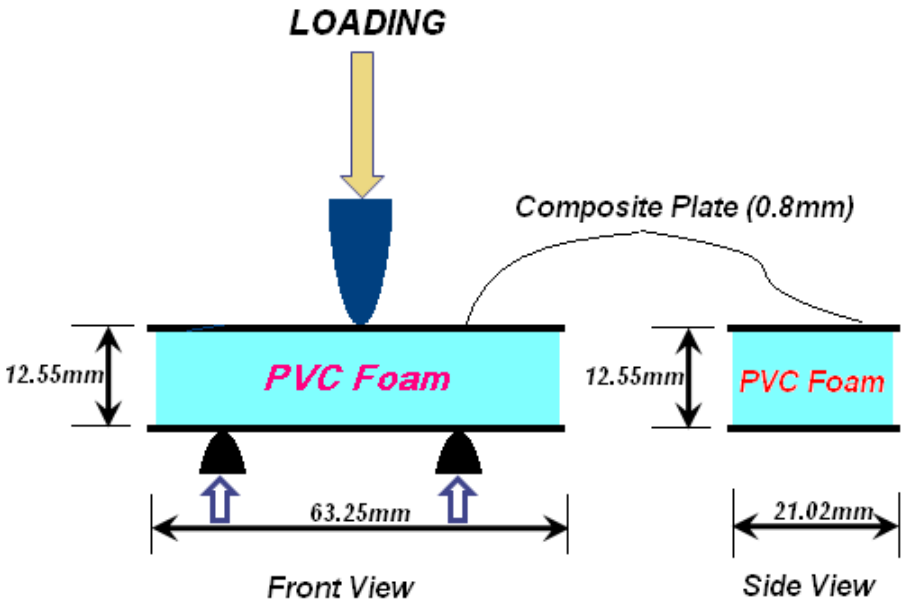

Fig 2.17 Geometry of sandwich beams with auxetic or conventional foam

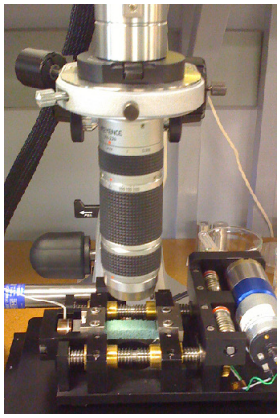

Fig 2.18 VHX-100 digital optical microscope

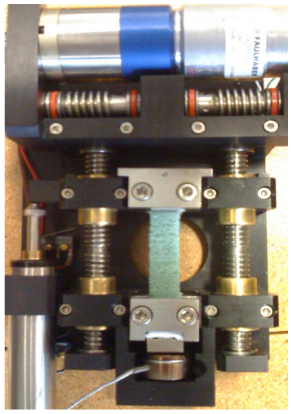

Fig 2.19 servo controlled Microtester

The VHX-100 digital optical microscope can record the entire loading process. The full video was captured and separated to single images by VirtualDub. Typically some of them were selected for analysis. The values of load can be read directly from the servo controlled microtester, and the cross section area of the specimen in the viewing area can be measured and calculated by Photoshop software. That is how the true stress be obtained.

2.4 Current Research and Tests

2.4.1 Sandwich Bending Test with Conventional and Auxetic Foam Core

Several sandwich beams with dimensions as depicted in Fig 2.17 were manufactured. Both the original conventional PVC foam and the fabricated auxetic foam were used as the core material. The beam subjected to three-point bending load, the distance between two supports is 45.4mm. The load was exerted on a punch via a hydraulic machine. The displacement was gauged by LVDT, which was attached onto the punch. The deflection curves under progressively increased load as shown in Fig 2.20. The red curve is the load-displacement relationship of auxetic foam, while the blue curve is the load-displacement relationship of conventional foam. It is seen that the deflection for the beam with auxetic foam core is markedly lower.

Failure behavior is presented as well. Compared with conventional foam which tends to be having shear failure of the core (A. Shukla), the sandwich beam with auxetic foam core failed at the face sheets first. The result shows that the auxetic foam enhance the failure properties of composites due to that auxetic foam allows the possibility of

maintaining the interface stiffer by higher shear modulus. The fracture result is shown in Fig 2.21.

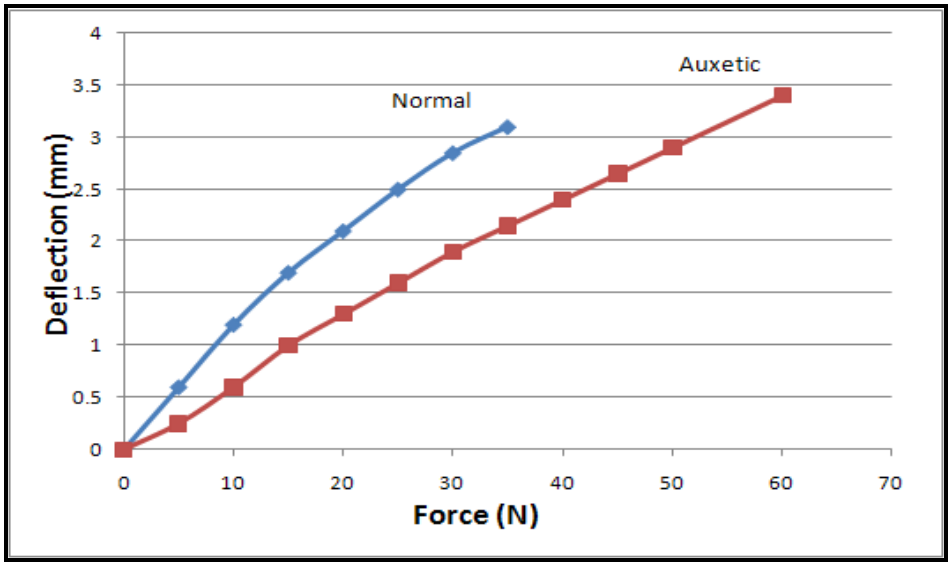

Fig 2.20 Deflection of the sandwich beam with auxetic PVC foam

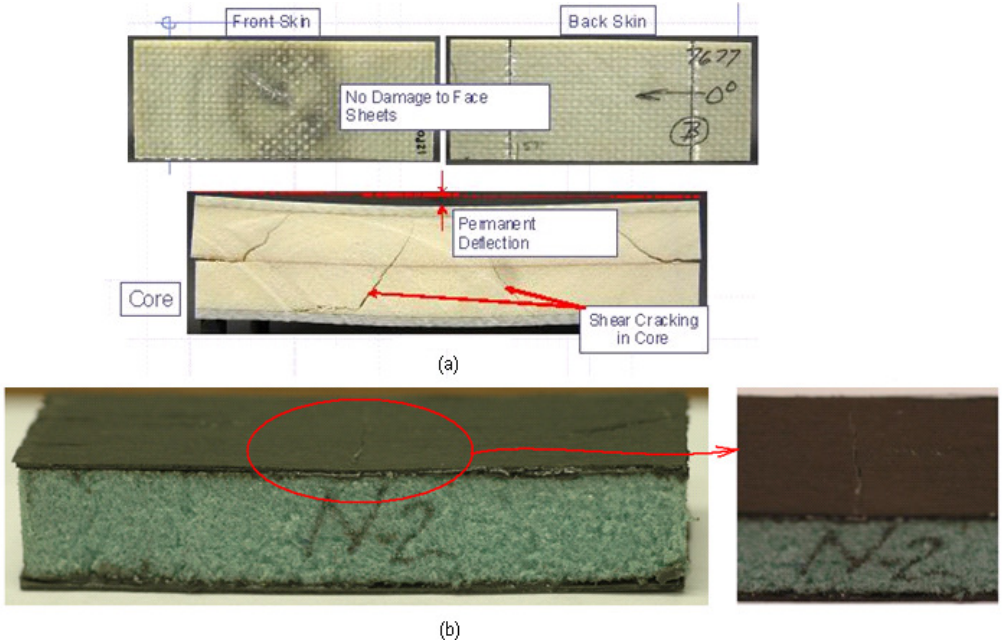

Fig 2.21 Fracture behavior under bending test (a) Conventional foam core; (b) Auxetic foam core

2.4.2 Cyclic Loading and Fatigue Test

Stress-strain loop of auxetic foam

Cyclic loading tests were performed on a number of auxetic foam specimens. The specimen underwent the following loading history: in the first cycle, the load started from 0, to the maximum value of 10N, and then went back to 0; in the second cycle, the load started from 0, to the maximum value of 15N, and then went back to 0. The next four cyclic loading, each increment of the maximum value is 5, progressively.

A typical result is shown in Fig 2.22. It is interesting to note that at earlier stages of loading the path of the stress-strain loop is counterclockwise whereas at the later stage the loop becomes clockwise as might expect. This is a rather interesting behavior that was not expected. For comparison, the same experiment was performed on the conventional foam. Another test on auxetic foam with the same loading history was carried out as well for easier comparison. The results are shown in Fig 2.23 and Fig 2.24.

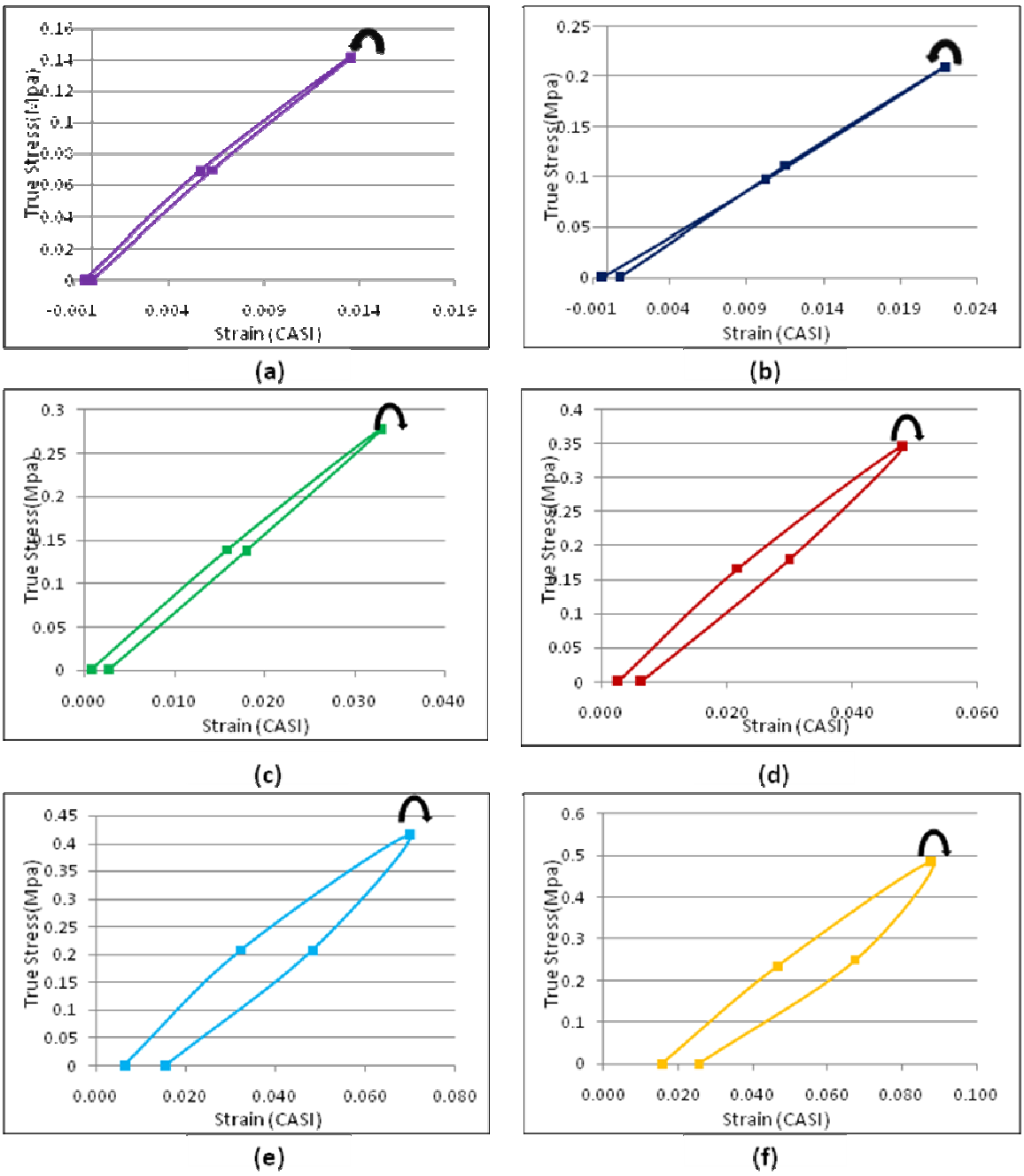

Fig 2.22 Stress-strain loops of the auxetic foam (a) Loading force from 0-10N-0; (b) Loading force from 0-15N-0; (c) Loading force from 0-20N-0; (d) Loading force from 0-25N-0; (e) Loading force from 0-30N-0; (f) Loading force from 0-35N-0

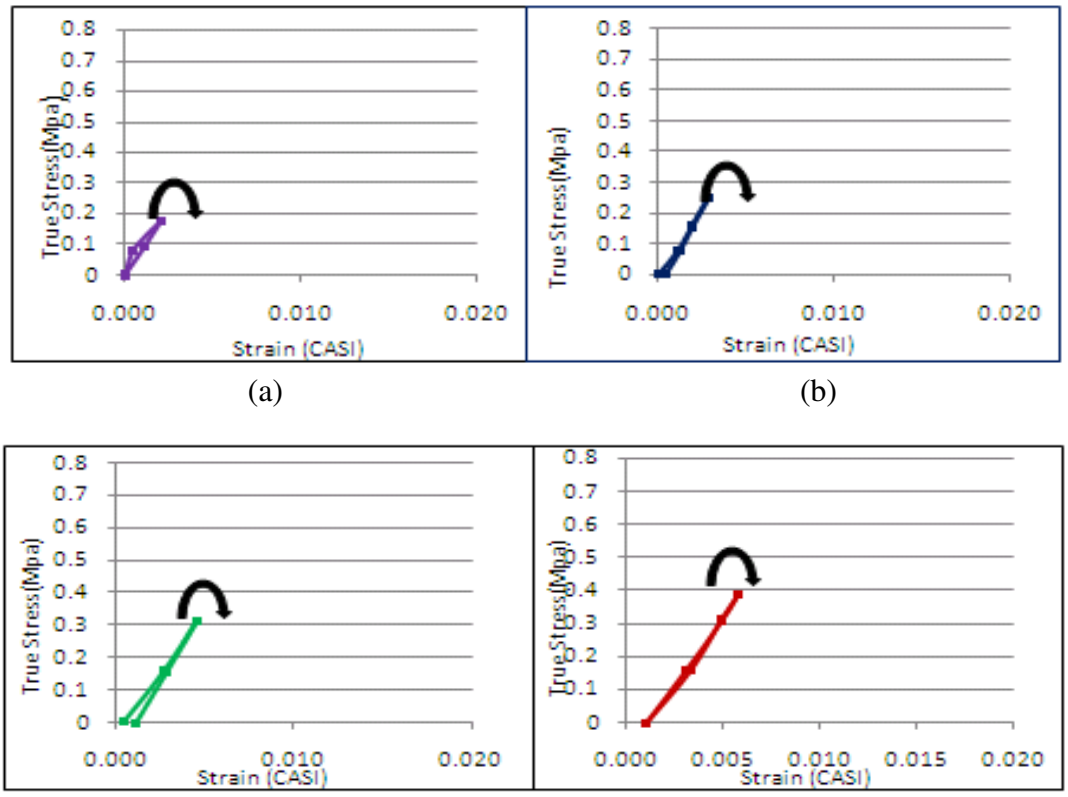

Fig 2.23 Stress-strain loop of the conventional foam (a) Loading force from 0-5N-0; (b) Loading force from 0-15N-0; (c) Loading force from 0-20N-0; (d) Loading force from 0-25N-0

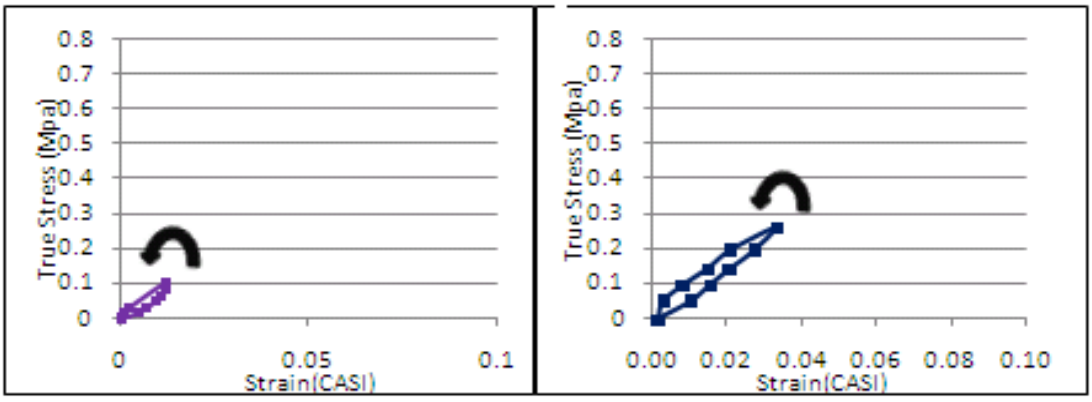

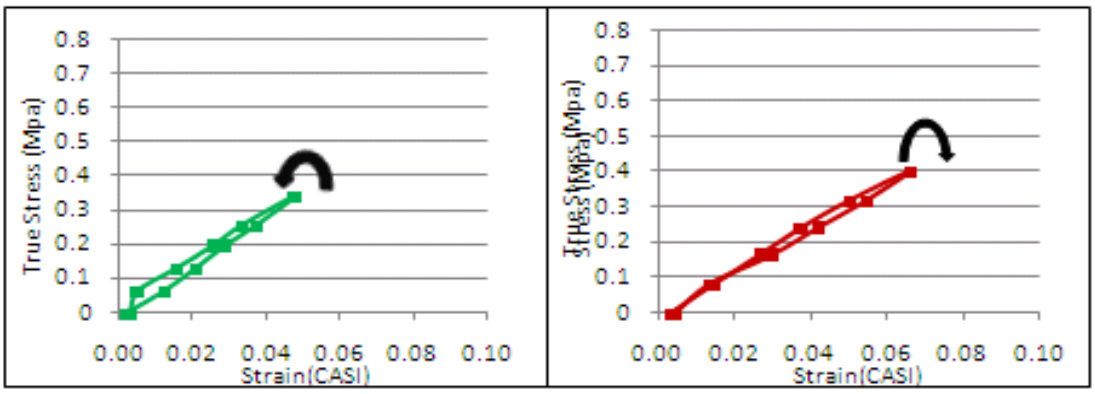

(c) (d)

Fig 2.24 Stress-strain loop of the auxetic foam (a) Loading force from 0-5N-0; (b) Loading force from 0-15N-0; (c) Loading force from 0-20N-0; (d) Loading force from 0-25N-0

As can be seen in Fig 2.23 and Fig 2.24, for the conventional foam, the stress-strain loop is always clockwise whereas for the auxetic foam it starts out counterclockwise and then changes to clockwise.

The stress-strain loop of auxetic foam is quite unusual. For a conventional material, the clockwise path of the stress-strain loop can be easily explainable. Upon loading the energy is stored in the materials, while upon unloading the energy is covered, but not 100% due to the effect of internal friction. In the case of the auxetic foam, at the early stage the energy recovered is larger than the energy provided. One possible explanation for this phenomenon maybe attributed to the fact that the original open foam cell is now converted into cells with re-entrant corners. There is residual strain stored inside the auxetic foam as a result. And this residual strain contributes to the energy dissipation of the cyclic loading process. Upon further loading, the re-entrant corners are straightened out, thus the material is essentially converted into conventional material. As a result, the clockwise loop prevails. The energy dissipation value as a function of applied

strain also was plotted as shown in Fig 2.25. Conclusion can be drawn that the higher auxeticity, the higher energy it can store.

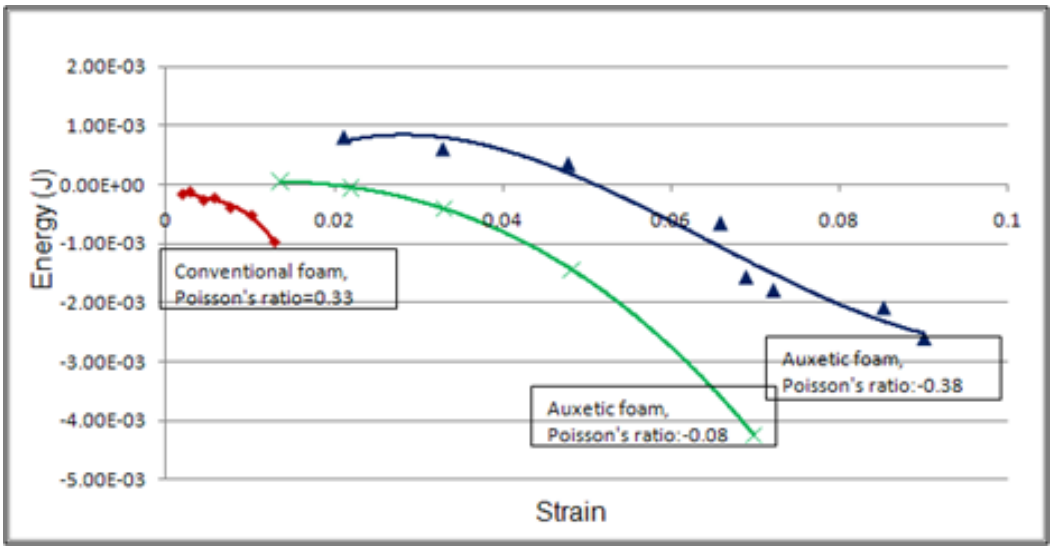

Fig 2.25 Energy dissipation as a function of the Poisson's ratio

Fatigue test

Fatigue test was also conducted by cyclic loading history to determine how the difference negative Poisson's ratio affects the life span of the auxetic foams. The size of the specimens is the same as in the previous test. The specimen was mounted onto the microtester, the loading speed was 2mm/min, and the experiments would not stop until the specimen was broken. The stiffness degradation with increase of loading cycles for two different Poisson's ratio's specimen is shown in Fig 2.26.

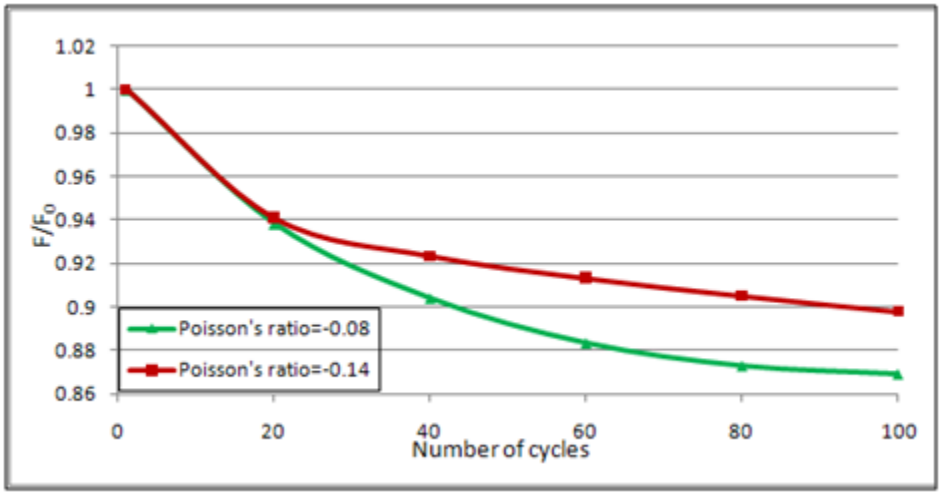

Fig 2.26 Stiffness degradation with increase of loading cycles with different Poisson's ratio

In Fig 2.26, F_0 is maximum load F obtained in the first cycle and F is maximum load obtained in the N cycle. Finally the auxetic foam was broken with average number of cycle 920 (Results vary from 810 to 1180) (Fig 2.27), compared to the conventional foam which was broken with average number of cycle 360 (Results vary from 230 to 430). The comparison shows that the auxetic foam has higher resilient and external force resistance over conventional foam.

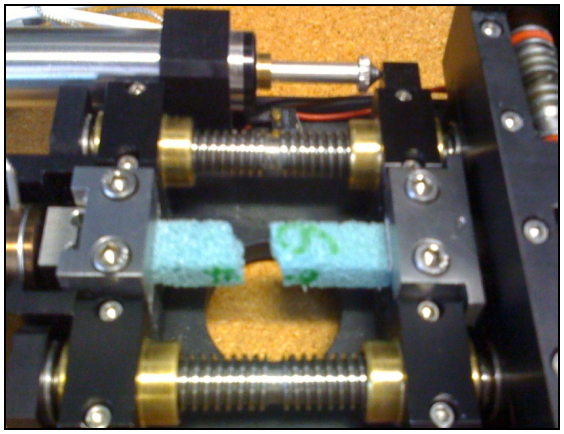

Fig 2.27 Auxetic specimen broken with number of cycle 920

2.5 Summary

In this section, conventional PVC foam has been successfully converted into auxetic foam via triaxial compression and heat treatment. The degree of auxeticity is a function of volume reduction was investigated as well: the higher the volume reduction, the larger the negative Poisson's effect is. Auxeticity materializes only after the volume reduction exceeds 50% approximately. Uniaxial test and shear test were conducted to determine the Young's module, and shear module. The results show that manufactured auxetic foams do have a larger Young's module and shear modulus. In the impact and indentation test, the results show that compared to the conventional foam, auxetic foam has higher resistance to indentation and low velocity damage. In the sandwich bending test with PVC foam core, sandwich panels with fiberglass face sheets and auxetic foam core can resist larger external forces with smaller deflection. Auxetic foam has a higher shear modulus thus minimizing one of the major failure modes of sandwich structures. These advantages and structural efficiency have been utilized to build high-speed naval patrol boats.

A few of mechanical behaviors of the auxetic foam under cyclic load are also investigated. Some interesting results on the stress-strain loops are found and analyzed. For conventional foam, upon loading the energy is stored in the materials, upon unloading the energy is covered, but not 100% due to internal friction. The path of the stress-strain loop is clockwise. For auxetic foam, at the early stage the energy recovered is larger than the energy provided. One plausibly explanation for this phenomenon maybe attributed to the fact that the original open foam cell is now converted into cells with re-entrant micro structures, which renders residual strain to be stored inside the auxetic foam

as a result. And this residual strain contributes to the energy dissipation of the cyclic loading process.

Upon the fatigue test under cyclic loading, for a prescribed strain, the stiffness of auxetic foam degradates when the number of cycles increases. Compared with the conventional foam, the auxetic foam shows higher resilient, external force resistance and higher life-span.

Chapter 3 Studies of a Wooden Bridge

3.1 Purpose of Study

Many bridges in this country are getting aged and need to be inspected and examined frequently. When a bridge is designed, the deformation patterns due to static loads are calculated carefully. However, as the structure ages due to corrosion and fatigue, the deflection patterns under load change. To maintain the state of health of a bridge can be ascertained by studying the deflection patterns periodically. Since currently, the inspection methods are low efficient, tedious and time consuming; it is impractical and very costly to inspect the entire bridge with instruments such as thermal imaging. In this thesis, Digital Speckle Photography (DSP) will be presented as an effective method for mapping the entire bridge deformation simultaneously in a single step. On the other hand, DSP can zoom to a local area and map the local deformation and strain in detail. The goal of this research is to study the deformation patterns of a bridge by DSP.

For short bridges, such as an overpass of a highway, a single digital camera (such as CCD or CMOS) camera will be sufficient. It should be situated as that a relatively normal view of the entire bridge can be obtained. A single white light source, such as a spotlight or a searchlight, is expanded using appropriate optics to illuminate the bridge from the side, which is to be painted with a thin coat of retro-reflective paint (e.g., Liquid reflector), described in the next section. A digital picture of the speckled surface of the bridge is taken when there is no traffic on the bridge. Subsequently, pictures are taken when the bridge is occupied by various amounts of traffic until the full load with bumper

to bumper cars, such as during the rush hours. Each subsequent picture is "compared" with the initial one and the CASI software is employed to calculate the displacement map of the entire bridge under various loading conditions.

3.2 Equipments and Procedures

For this study a wooden truss bridge using standard pine wood strips purchased from Home Depot is built. The total length of the bridge is 10ft, the width is 2ft and the height is 1.25ft. The dimensions of the bridge are shown in Fig 3.1 and the actual model is shown in Fig 3.2.

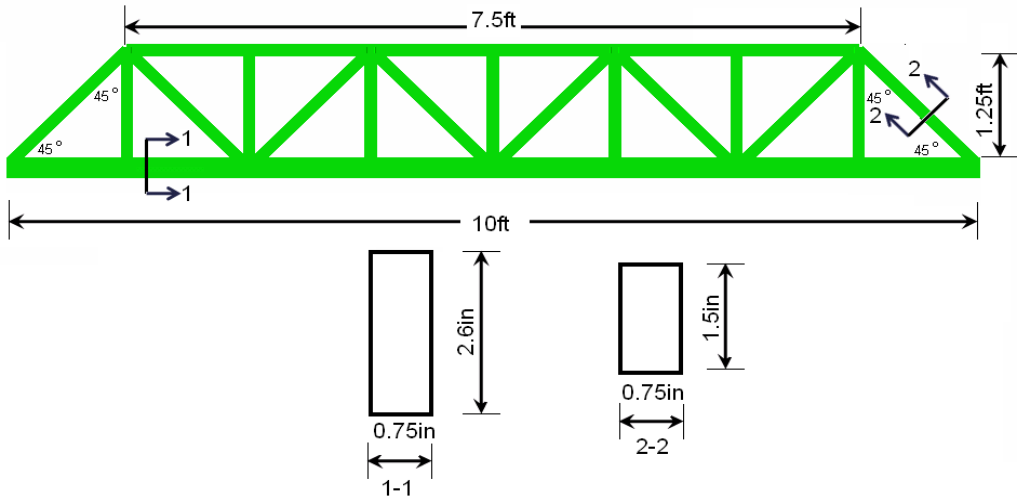

Fig 3.1 Sketch of the model wood bridge

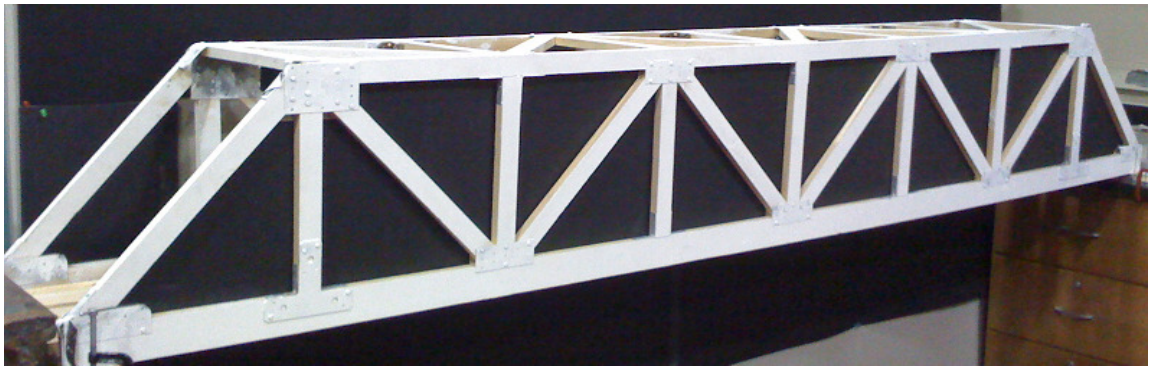

Fig 3.2 Picture of the actual model wood bridge

One surface of the bridge that is facing the camera is treated with a thin coat of retro-reflective paint which contains of imbedded minute glass beads of about 20-40μm is size. The glass bead has an index of refraction such that when a beam of light impinges upon it, the total internal reflection will redirect the beam to where it comes from with minimum scattering as schematically shown in Fig 3.3.

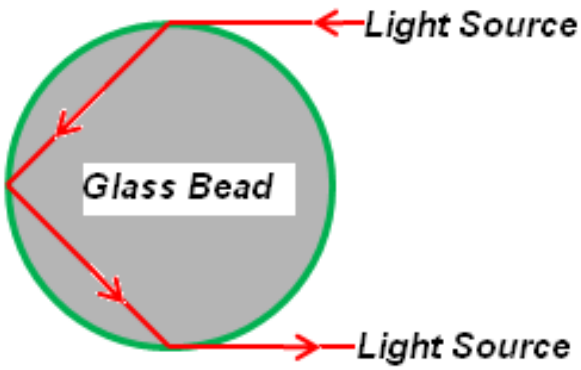

Fig 3.3 A glass bead redirects light back towards the source

So that the totality of the painted surface presents itself as having a speckle pattern when viewed from a direction very close to the light source. Thus a surface with such paint reflects light efficiently towards the light source. As a result one can use a relatively small light source to illuminate a large structure such as a bridge and obtain

good speckle patterns for subsequent processing. The experimental setup for the experiment is shown in Fig 3.4.

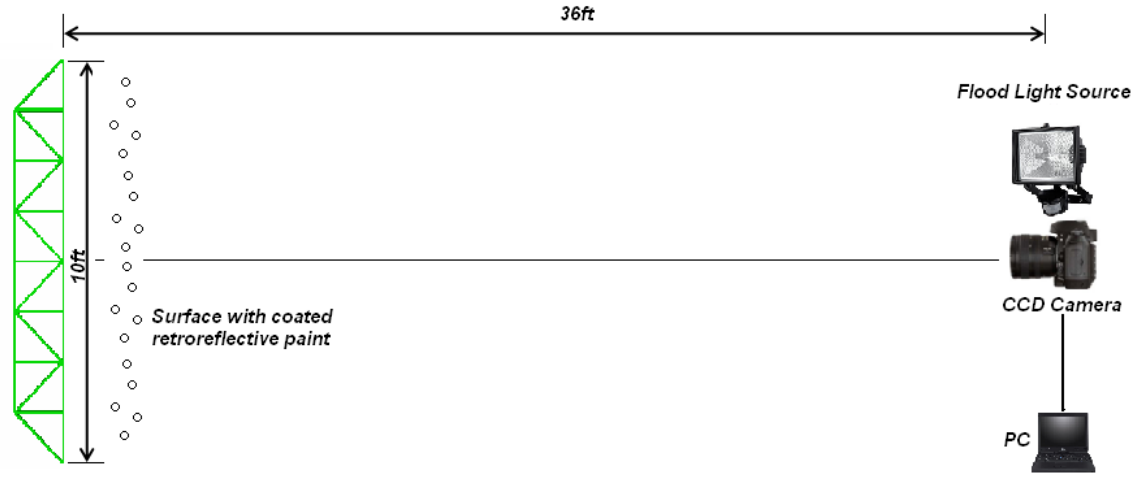

(a)

(b)

(c)

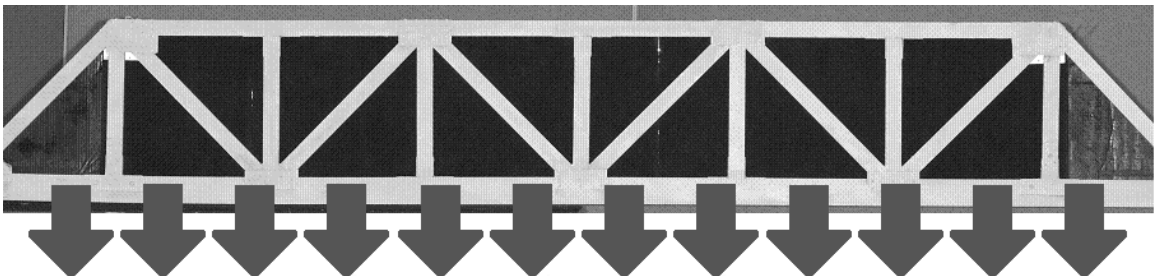

(d)

Fig 3.4 Experimental setup for full field bridge deformation mapping (a) Sketch of the experimental setup; (b) Picture of the experimental setup; (c) Distribution of load from sand bags; (d) Sketch of load direction

In the experiment, a digital camera (Nikon Model D70) with 3008×2000 pixels resolution is used to record the speckled wood bridge, the camera with its optical axis essentially normal to the beam is situated some 36ft away (Fig 3.4 a) and is connected with PC. One flood lights (300w type T3 floodlight) are used to illuminate the wood bridge (Fig 3.4 b). The two items are fairly close to each other so that the camera can receive the narrowly retro-reflected light for the maximum effect. The load is applied by piling 50 lbs sand bags on the top of the bridge deck All static loads for the structure is about 600 lbs (Fig 4.4c, d). The face of the bridge that is coated with retro-reflective paint is photographed by the digital camera and the each digital image of the bridge is subdivided into subimages of 128 ×128 pixel arrays and then “compared” using the CASI software described in the previous section.

3.3 Results and Discussions

3.3.1 Full-Field Mapping of Global Deformation

Two pictures were taken, which covered the whole image of the bridge, one is before the deformation and another is after the deformation. In order to analyzing these two image in CASI, two pictures should have the same sizes and with gray color. Then

two digitalized speckle patterns were “compared” or “subtracted” in the CASI program. The results are shown in Fig 3.5 when the total load is 400 lbs.

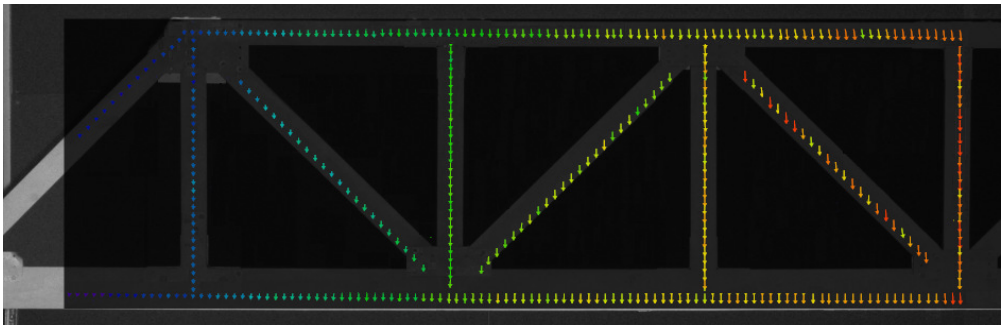

(a)

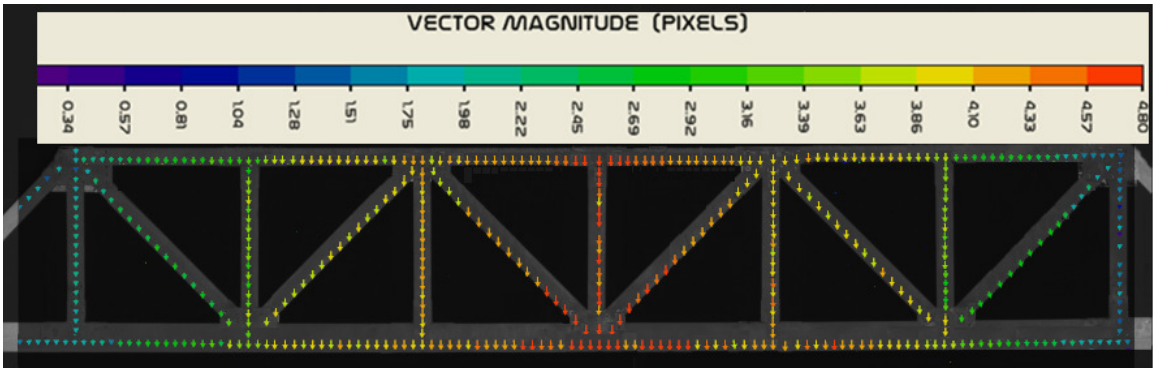

(b)

Fig 3.5 Displacement vectors depicting the reflection of the beam under static weight for the (a) half bridge and (b) entire bridge

The result in Fig 3.5 shows the half and entire bridge to demonstrate not only the technique’s high spatial resolution, but also the value of the deflection. The vectors represent quantitatively the magnitude and direction of the beam at each and every point where the vector is located. The magnitude of the deflection is pseudo colored as depicted in the picture next to the beam. It is seen that it varies from zero at the left and the right side supported, to 4.8 pixels (here, 4.8 pixels equals to 3.48mm) at the center of the processed region of the bridge. The strain distribution will be calculated and demonstrated in a next section.

3.3.2 Finite Element Analysis of Global Deformation

Finite element analysis of the bridge using the ABAQUS 6.8-1 software has been performed. The three dimensional geometry is shown in Fig 3.6.

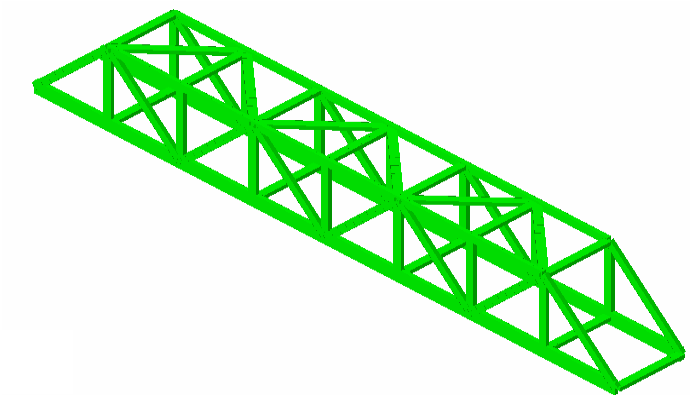

Fig 3.6 Geometry model in ABAQUS

The Young's modulus of pine wood is 11.6Gpa, Poisson's ratio is 0.3, and density is 562 kg /m^3. The deflection analysis is a linear static step. The distributed load is 400lb, the boundary conditions are defined as U1, U2, U3 are zero, which means all the translation degree of freedoms will be fixed, at the two ends of the bridge representing a pin support. The element is 2-node linear beam in space. In order to simulate the shear flexible effect, Timoshenko beam element is selected and the element type is B31. Abaqus/Standard solver is used and the result of the bridge deflection is compared with CASI's as shown in Fig 3.7. In Fig 3.7, it can be noticed that these two results are reasonably compatible.

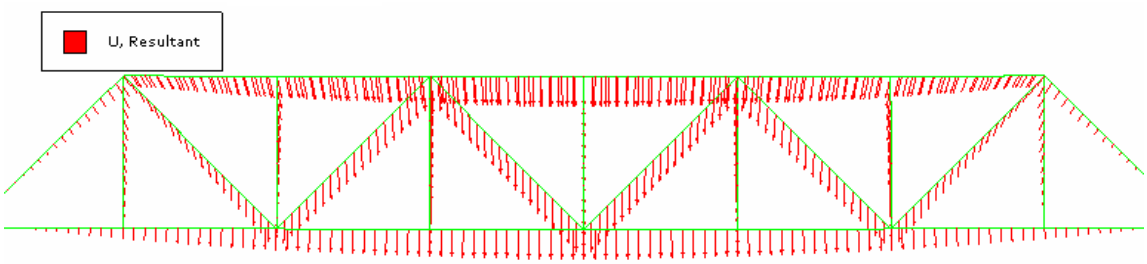

(a)

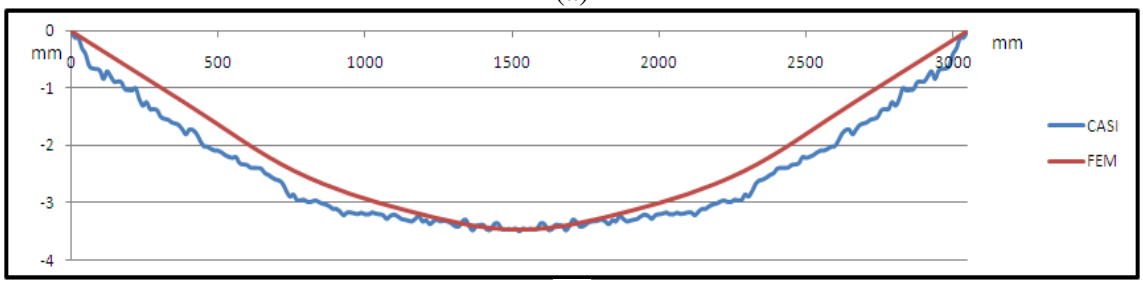

(b)

Fig 3.7 (a) Deflection vectors of the bridge by FEA, (b) Bridge main beam deflection from CASI and FEA

3.3.3 Local Mapping of Strain Concentration Areas in a Bridge

Bridge failure usually starts locally. It is paramount that critical regions be identified and monitored for stress-strain concentrations. From the theoretical calculation or field observation using the systems described in the previous section, one can determine the regions of stress/strain concentration or the likelihood of stress/strain concentration. Once a region (or regions) is identified, the speckle technique can be deployed to monitor the involution of the local strain field. Strain concentration usually leads to crack initiation which may grow into critical size resulting in catastrophic failure.

The example shown in Fig 3.8 is that of central area where the maximum deflection can be obtained in the bridge under static loading equals 400 lbs. For the beam structure under bending condition, the area above the neutral axis is compressive, and under the neutral axis is tensile. In the thesis, the tensile strain will be calculated both by CASI and strain indicator.

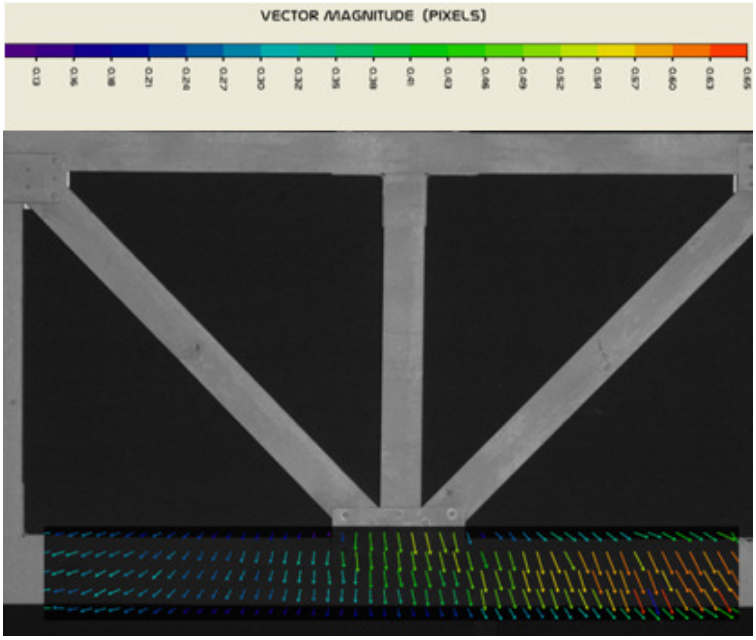

Fig 3.8 Total displacement vector distribution of the main beam under 400 lbs total load

Meanwhile, four strain gages are mounted onto the surface of the main beam to calculate the strain directly by strain indicator (Fig 3.9).

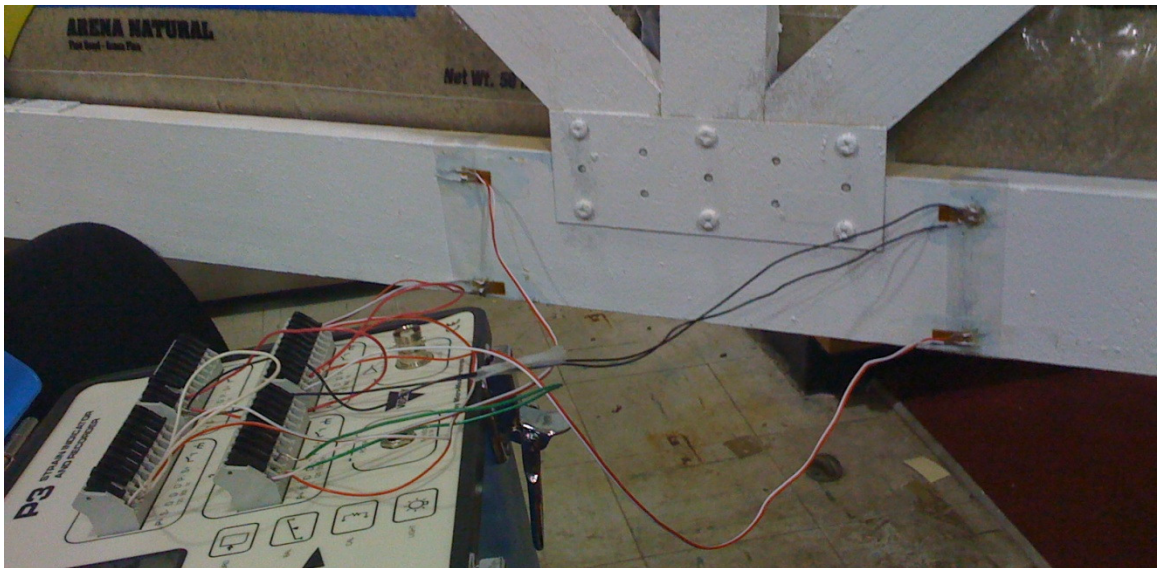

Fig 3.9 Strain gage location on the main beam

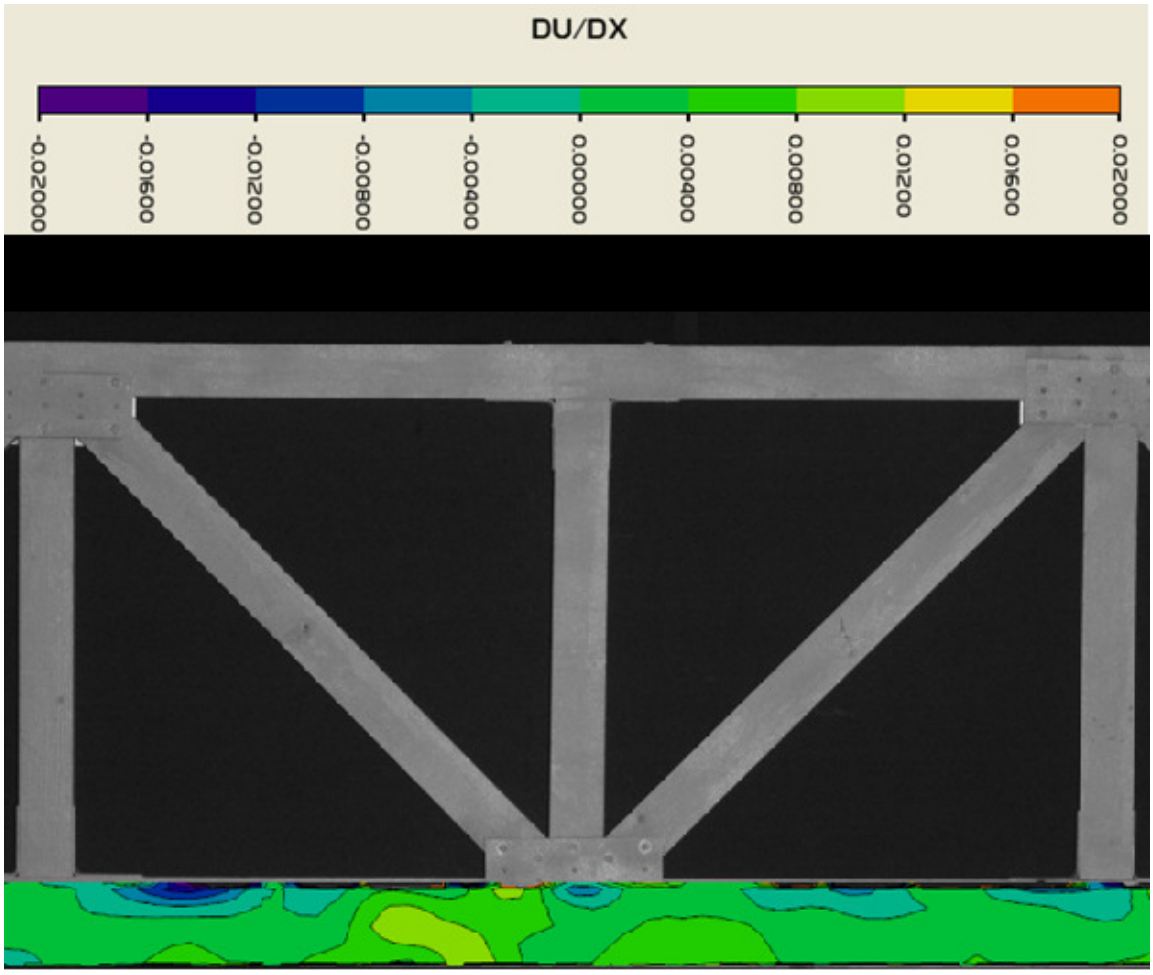

Fig 3.10 Strain distribution of the main beam as obtained by DSP techniques

Fig 3.10 shows the strain distribution of the main beam. It is noted that the strain distribution indicates that while the entire beam is mostly under tension, there are zones of compression on the top of the beam are wanted predict. The strain gage results are as follow -12 mε (top left), 16 mε (bottom left), -10 mε (top right) and 14 mε (bottom right). Reasonable agreement is obtained.

3.4 Summary

DSP technique can be applied to monitor the deflection and strain distribution of 10ft model wood beam. It can be noticed that the strain distribution of CASI is pretty

precise be mean of comparing with the strain gages. On the other hand, the compression of the CASI result with that of the FEM is reasonable. Some discrepancies are near the center of the main beam. In the CASI result, some oscillation is shown, this is because the data obtained from CASI is rigid connected directly without any smooth. Another reason for the discrepancy is that in the FEM simulation, the mechanical properties of pine wood are not tested with full accuracy. Since wood may be described as an orthotropic material, it has unique and independent mechanical properties in the directions of three mutually perpendicular axes: longitudinal, radial and tangential. In order to measure the accurate elastic properties, a series of experiments for testing the wood properties need be conducted. However, it is believed this technique can be applied to real bridges and other infrastructures with proper modification of the proposed system.

Chapter 4 Conclusions and Future Work

Digital Speckle Photography (DSP) technique has been applied to the study on the behavior of two-dimensional speckles in the presence of two different structures' surfaces. The surface roughness of the foam served as an ideal speckle patterns. Two pictures, before and after the deformation of the surfaces, are digitally subtracted through the Computer Aided Speckle Interferometry (CASI) method, and the displacement, as well as the strain fields are obtained.

In this thesis, two studies are presented by using DSP as a key method to investigate the mechanical properties of material and structure. The results show that DSP is a good technique for full mapping deformation measurement. Additionally, DSP provides higher accuracy of measurement. For example, when gauging the total displacement of coupon specimen, using clip or LVDT will not reveal whether or not the specimen is uniformly deformed due to local errors of measurements, but these errors can be avoid using DSP method.

Auxetic foam demonstrates the fascinating property of getting expending when stretched, contracting when compressed. In this thesis, auxetic PVC foam has been successfully manufactured, its advanced mechanical properties are tested and investigated based on various mechanical experiments. When compared with conventional foam, auxetic foam has much better mechanical properties; it provides a potential new material for sandwich plate constructions with higher rigidity and stronger failure resistance. Nowadays, it has attracted many scientists' concerns on the auxetic materials due to its unique behavior. Much attempt has been made to explore not only materials with

auxeticity, the mechanics from which the property comes and the manufacturing methods, but also the mechanical, indention, deformation, or viscoelastic properties and other functional characteristics result from the auxeticity. Furthermore, the successful development of auxetic material leads to new materials with extreme properties such as high strength and modulus. With these fundamental researches, the applications of auxetic materials show a very bright potential.

Moreover, static deflection analysis of a wood bridge by DSP has been analyzed. CASI has been proved to be a very powerful tool for determining displacement. The results of displacement field in CASI has a good compatible with Finite Element Analysis, the results of local strain field has a good agreement with strain gage. If displacement is known, a vector field of structure can be obtained. This technique is full field view thus quantitative and qualitative information can be obtained and it can also be applied to bridges that experience vibration. By studying the changes of the displacement field over periods of time, the state of health of a bridge can be detected and evaluated.

For the future work, three-dimensional full field mapping of the wood bridge's deformation should be carried out. Meanwhile, The DSP technique can also be applied to bridges that experience vibration. A preliminary test on applying this technique to capture the dynamic response of a bridge needs to be investigated, such as, during a heavy truck moving at a relatively high speed or during a wind storm. The experiment is to carry out a suddenly dropped weight on the beam. The aim is to see if the Digital Speckle Photography can be applied to capturing the oscillation of the beam quantitatively. Such a situation was investigated in a previous paper by the seminar author [39]. Both the in-plane and out-of-plane oscillation of the bridge can be detected and quantified [39]. There are

situations when one would wish to investigate many local deformations such as those in gusset plates. The DSP technique can also be applied simply by zoom in with the digital camera. In extreme cases, optical microscope or even scanning electron microscope can be used as the recording device [39, 40].

Bibliography

[1] **Lakes, R.S.** "Foam structures with a negative Poisson's ratio", *Science*, 1987, **235**:1038-1040

[2] **Evans, K.E., "**Auxetic Polymers: a New Range of Materials", Endeavour (UK), *New Series*, 1991, **15**(4):170-174

[3] **Chan, N.** and **Evans, K. E.** "Fabrication methods for auxetic foams", *J. Mater. Sci.* 1997, **32**(22):5945–5953.

[4] **Evans, K. E.** "Tailoring the Poisson's ratio", *Chem. Ind.* 1990, **20**:654–657.

[5] **Chen, C. P.** and **Lakes, R. S.** "Micromechanical analysis of dynamic behavior of conventional and negative Poisson's ratio foams", *J. Eng. Mater. Technol.*, 1996, **118**(3):285–288.

[6] **Alderson, A.** and **Alderson, K.L.** "Auxetic materials", *Aerospace Engineering*, 2007, **221**: G-J.

[7] **Yang, W., Li, Z. M., Shi, W., Xie, B.H.** and **Yang, M.B**. "Review on auxetic materials", J*our. Mater. Sc., 2004,* **39**(10):3269 – 3279

[8] **Scarpa, F., Panayiotou, P. and Tomlinson, G.** "**Numerical and experimental uniaxial loading on in-plane auxetic honeycombs**", *Journal of Strain Analysis and Engineering Design*, 2000, **35**(5):383-388.

[9] **Friis, E. A., Lakes, R. S., and Park, J. B.** "Negative Poisson's ratio polymeric and metallic materials", *Journal of Materials Science*. 1988, **23**:4406-4414.

[10] **Chen, C. P. and Lakes, R. S.,** "Dynamic wave dispersion and loss properties of conventional and negative Poisson's ratio polymeric cellular materials", *Cellular Polymers*, 1989, **8**(5):343-359.

[11] **Lakes, R. S.,** "Experimental micro mechanics methods for conventional and negative Poisson's ratio cellular solids as Cosserat continua", *J. Engineering Materials and Technology*, 1991, **113**:148-155.

[12] **Chiang, F. P. and Uzer, G.,** "Mapping full field deformation of auxetic foam using digital speckle photography", *Physica Status Solidi (b)*, 2008, **245(11)**:2391-2394

[13] ***Peters, W. H.*** and ***Ranson, W. F.,*** "Digital imaging techniques in experimental mechanics," *Opt. Eng.* 1982, **21**:427-431.

[14] **Chiang, F.P., Uzer, G.,** and **Krukenkamp, I.B.**, "Measuring Shape and Surface Strain in Curved Objects Using Digital Speckle Photography and Gap Effect," *Strain- An Int. J. for Experimental Mechanics*, 2008, **44(5)**:409-416.

[15] **Chiang, F.P.** and **Asundi, A.**, "White light speckle method of experimental strain analysis," *Applied Optics.*, 1979, **18(4)**:409-411.

[16] **Chen, D.J.** and **Chiang, F.P.** "Range of measurement of computer aided speckle interferometry (CASI)," *Proc. 2nd Int. Conf. On Photomechanics and Speckle Metrology,* San Diego, CA, 1554A, July 22-26, 1991, 922-931.

[17] **Burch, P.G.** and **Migeon, C.J.** "Systemic Absorption of Topical Steroids" *Arch Ophthalmol.* 1968, 79(2):174-176.

[18] **Jones, R.** and **Wykes, C.** "Holographic and Speckle Interferometry". *Journal of Applied Mathematics and Mechanics.*1985, **65(2)**:70.

[19] **Li, D.W.** and **Chiang, F.P.** "Effect of magnification change in laser speckle interferometry," *J. of Optical Soc. of America,* 1978, **68(12)**:1742-1748.

[20] **Chiang, F.P.** and **Asundi, A.** "Perspective effect in white light speckle method," *Applied Optics*, 1982, **21(11)**:1887-1888.

[21] **Jin, F.** and **Chiang, F.P.** "A New Technique Using Digital Speckle Correlation for Nondestructive Inspection of Corrosion", *Material Evaluation*, 1997, **55(7)**:813-816.

[22] **Chiang, F.P.** "Super-resolution digital speckle photography for micro/nano measurements," *Optics and Lasers in Engineering,* 2009, **47**:274-279.

[23] **Chen, D.J.** and **Chiang, F.P.** "Notch tip strain field by CASI," *Proc. 2nd Int. Conf. On Photomechanics and Speckle Metrology*, San Diego, CA, 1554A, 1991, July 22-26.

[24] **Chen, D.J.** and **Chiang, F.P.** "Computer aided speckle interferometry using spectral amplitude fringes," *Applied Optics*, 1993, **3(2):**225-236.

[25] **Sjodahl, M.** and **Benckert, L.R.** "Electronic speckle photography: analysis of an algorithm giving the displacement with subpixel accuracy" 1993, *Applied Optics*, **32(13)**:2278-2284.

[26] Rastogi, P.K. "Digital speckle pattern interferometry and related techniques", 2001, Wiley, ISBN: 978-0-471-49052-4.

[27] **Chen, D.J., Chiang, F.P., Tan, Y.S.,** and **Don, H.S.,** "Digital speckle displacement measurement using complex spectrum method," *Applied Optics*, 1993, **32**:1839-1849.

[28] **Alderson, A., Rasburn, J.,** and **Evans, K. E**. "Mass transport properties of auxetic (negative Poisson's ratio) foams". *Phys. Status Solidi* B, 2007, **244(3)**:817–827.

[29] Wiki, 2010, *http://en.wikipedia.org/wiki/Umbrella*

[30] **Lakes, R.S.,** and **Elm, K. J.** "Material structure for attaining pure Poisson-shearing" *Compos. Master.,* 1993, **27**:1193-1202

[31] **Scarpa, F., Yates, J. R., Ciffo, L. G.,** and **Patsias, S.** "Dynamic crushing of auxetic open-cell polyurethane foam". *Proc IME CJ Mech Eng Sci.*, **216**:1153-1156.

[32] **Whitty, J.P.M., Alderson, A., Myler, P.,** and **Kandola, B**. "Towards the design of sandwich panel composites with enhanced mechanical and thermal properties by variation of the in-plane Poisson's ratios". *Compos. A, Appl. Sci. Manuf.,* 2003, **34(6)**:525-534.

[33] **Vinson JR, Rajapakse, V., JR** and **Carlsson, Y. LA** (Eds.). "Proceedings of the Sixth International Conference on Sandwich Structures". Proceedings of 6th International Conference Sandwich Structures, Ft. Lauderdale, FL, 03/30-04/02, 2003.

[34] **Chiang, F.P.,** and **Ding, Y.,** "Size Effect on Stress-Strain Relation of Neat Polyurethane Foam," *Composite Part B Engineering,* 2008, **39**:42-49.

[35] NCHRP SYNTHESIS 375, "Bridge Inspection Practices". Transportation Research Board of the National Academies.

[36] **Chiang, F.P.** and **Yu, J.D.** "Full Field Mapping of Bridge Deformation Using Digital Speckle Photography," Proc. Of 5th International Conference on Bridge Maintenance, Safety and Management, Philadelphia, PA, July 11-15, 2010.

[37] **Chiang, F.P., Ding, Y.,** and **Uzer, G.,** 2008. "Auxetic Foam as a core material for Sandwich Panels," *Proc. of 8th International Conference on Sandwich Structures*, Porto, Portugal, May 6-8, 2008.

[38] **Stott, P.J, Mitchell, R., Alderson, K.,** and **Alderson, A.,** "A growth industry". *Materials World*, 2000, **8**:12-14.

[39] **Chiang, F.P.** "Remote Sensing of Bridge Oscillation using Digital Speckle Photography," *Proc. of 5th New York City Bridge Conference*, New York City, New York, August 17-18, 2009.

[40] **Chiang, F. P.,** "Remote sensing of bridge oscillation using digital speckle photography", *Optics & Laser in Engineering,* 2009.

[41] **Chiang, F. P.,** and **Lin, C. J.,** "Stress analysis of in-plane vibration of 2D structure by a laser speckle method," *Applied Optics*, 1980, **19(16)**: 2705-2708.

[42] **Chiang, F. P.,** and **Keene, L.,** "Real-time anti-node visualization of vibrating distributed systems in noisy environments using defocused laser speckle contrast analysis," *Journal of Sound and Vibration*, 2008, **320(3)**: 472-4744.

[43] **Chiang, F. P.** and **Gupta, P. K.,** "Laser speckle interferometry applied to studying transient vibrations of a cantilever beam," *J. of Sound and Vibration,* 1989, **133(2)**:251-259.

[44] **Johansson, E. L.,** "Digital speckle photography and digital holography for the study of transparent media". Doctoral thesis. Department of Applied Physics and Mechanical Engineering. Division of Experimental Mechanics. Lulea University of Technology. 2007

[45] **Singh, R. P.,** and **A. Shukla**, "Characterization of Isochromatic Fringe Patterns for a Dynamically Propagating Interface Crack," *International Journal of Fracture*, 1996, **76**:293–310